https://doi.org/10.5194/essd-2026-216
Preprint. Discussion started: 28 April 2026

Open Access Earth System Science Data Discussions

A global high-resolution dataset of snowmelt runoff onset timing from Sentinel-1 SAR, 2015-2024

Eric Gagliano[1], David Shean[1], Scott Henderson[2,3]

[1]Department of Civil and Environmental Engineering, University of Washington, Seattle, WA, 98195, USA
[2]Department of Earth and Space Sciences, University of Washington, Seattle, WA, 98195, USA
[3]eScience Institute, University of Washington, Seattle, WA, 98195, USA

Correspondence to: Eric Gagliano (egagli@uw.edu)

Abstract. Snowmelt runoff onset timing represents a critical hydrological parameter, particularly in mountainous regions where seasonal snow serves as a natural reservoir for downstream water resources. Despite this importance, high-resolution observations of snowmelt runoff onset across complex terrain are limited, due to challenges from sparse in situ monitoring networks, intermittent optical remote sensing data, and coarse passive microwave remote sensing data. To address this gap, we prepared a global snowmelt runoff onset timing dataset (https://doi.org/10.5281/zenodo.16953614) for the 10-year period spanning 2015 to 2024, with 80-meter spatial resolution and 9.2-day average temporal resolution. We created this dataset by identifying backscatter minima indicative of runoff onset in a time series of Sentinel-1 C-band SAR images, with detection constrained by a custom MODIS-derived snow phenology dataset. We validated our dataset using in situ snow pillow estimates of runoff onset from 735 automated weather stations in the Western United States, finding a median timing difference of -1.0 days and a median absolute deviation of 9.0 days. The local agreement between our runoff onset estimates and snow pillow runoff onset estimates varies with site-specific variables like forest cover fraction, SWE, and dataset temporal resolution. We characterized these dependencies to provide empirically-derived thresholds for quality filtering as well as guidance for interpretation and use of our products. The dataset includes global annual runoff onset products for each water year, annual local temporal resolution products for each water year, and 10-year composites of median runoff onset, median absolute deviation, and local temporal resolution. This unique combination of high spatial resolution, global coverage, and decade-long temporal coverage provides unprecedented detail for the study of snowmelt runoff onset across snow-covered regions. Our snowmelt runoff onset dataset enables an improved understanding of mountain hydrological processes and informs water resource management in snow-dominated watersheds.

1 Introduction

Snow plays a crucial role in the global water cycle and climate system, and more than one-sixth of the world's population relies on meltwater from seasonal snow and glaciers (Barnett et al., 2005). This dependence is particularly pronounced in mountainous regions, where seasonal snowpack acts as a natural reservoir, storing water as snow in the winter and gradually releasing it during spring and summer months. Critically, snowmelt runoff onset marks the beginning of increased water

https://doi.org/10.5194/essd-2026-216
Preprint. Discussion started: 28 April 2026

availability, initiating the annual hydrologic pulse that sustains downstream ecosystems and human water needs during the warmer months (Dingman, 2015). This snowpack-scale process is distinct from basin-scale streamflow generation – the streamflow response at basin outlets typically follows snowmelt runoff onset by days to weeks depending on basin characteristics such as topography, vegetation, bedrock permeability, groundwater storage capacity, soil moisture conditions, and hillslope and groundwater travel times (Brooks et al., 2025; Lowry et al., 2010).

Beyond its hydrological significance, snowmelt timing also serves as a key indicator of regional climate change, potentially manifesting before other environmental indicators (Dudley et al., 2017). As a process, snowmelt timing is highly sensitive to temperature and precipitation variations, and shifts in the spatial distribution of snowmelt over time provide tangible evidence of changing climate conditions. In recent decades, climate change has driven spatially heterogeneous trends in the timing and spatial distribution of global snow accumulation and snowmelt that vary in direction (earlier vs. later) and magnitude across climatic and geographic settings (Ismail et al., 2023; Royer et al., 2021; Yang et al., 2022). These changes have far-reaching consequences for water security, agricultural productivity, and ecosystem health in snow-dominated regions and beyond (Qin et al., 2022).

Traditional methods for monitoring snowmelt, such as in situ measurements from snow courses and snow pillows (Cowherd et al., 2024; Lundquist et al., 2004), provide valuable point data but require labor-intensive collection that precludes the spatial coverage necessary for regional and global analysis. Snow pillows can be used to relate decreases in SWE to melt occurrence, but do not directly measure the liquid water content of the snowpack. Optical remote sensing data from platforms like Landsat, Sentinel-2, and MODIS can provide observations of fractional snow-covered area with broad spatial coverage, but these remote sensing approaches only indirectly indicate melt occurrence through decreases in snow cover over time, with additional challenges due to persistent cloud cover during critical melt periods (Awasthi & Varade, 2021). Passive microwave sensors have been used for large-scale snowmelt detection (Mioduszewski et al., 2015; Zheng et al., 2022), but are limited by very coarse spatial resolution (typically 25 km) that fails to capture snowmelt variability in the characteristically complex, mountainous terrain of snow-dominated regions.

Synthetic Aperture Radar (SAR) overcomes many of these limitations due to its all-weather imaging capability, high spatial resolution, and sensitivity to liquid water content in snowpack (Rott & Nagler, 1995; Tsai et al., 2019). The European Space Agency's Sentinel-1 C-band SAR mission is particularly useful for snowmelt monitoring due to its global coverage and frequent (often 6- or 12-day) exact repeat interval. When snow is dry, C-band radar can penetrate through the entire snowpack (up to ~20 m), with backscatter dominated by the snow-ground interface (Mätzler, 1987; Nagler et al., 2016). However, the presence of liquid water dramatically alters the dielectric properties of snow, causing greater absorption of C-band radiation, resulting in shallow penetration depth (~5-10 cm), and consequently, a significant decrease in backscatter (Lund et al., 2020; Nagler, 1996).

Studies of C-band SAR backscatter time series have established that the minimum backscatter amplitude coincides with the transition from the ripening phase to the runoff phase of snowmelt (Darychuk et al., 2023; Gagliano et al., 2023; Lund et al., 2022; Marin et al., 2020). Carletti et al. (2025) provided a more rigorous physical understanding of the

https://doi.org/10.5194/essd-2026-216
Preprint. Discussion started: 28 April 2026

relationship between this characteristic backscatter minimum and runoff onset, combining high-resolution field measurements and radiative transfer modeling. They demonstrated that the decrease in backscatter to the characteristic minimum is caused by signal absorption from increasing liquid water content, while the subsequent post-minimum backscatter increase is controlled by evolving snow surface roughness during the runoff phase. Importantly, Carletti et al. (2025) emphasized that rather than directly detecting the initiation of runoff onset, the backscatter minimum is caused by the complex interplay of these factors when the snowpack is already isothermal and likely releasing water. Despite these complexities at the process scale, this relationship between backscatter minimum and runoff onset timing has been validated in diverse mountain environments against various reference measurements, including snow pillows at automated weather stations (Darychuk et al., 2023; Gagliano et al., 2023; Gao & Ma, 2024; Marin et al., 2020), soil moisture pulses at automated weather stations (Detre et al., 2025), snow pit measurements (Lund et al., 2022; Rickenbaugh et al., 2026), a C-band SAR tower-based study (Brangers et al., 2024), and streamflow observations (Gagliano et al., 2023; Lund et al., 2022; Rickenbaugh et al., 2026).

However, the complexities revealed by Carletti et al. (2025) highlight the need for improved methodological approaches that can robustly detect snowmelt runoff onset across diverse environmental conditions. In previous work, we developed such an approach by integrating all available Sentinel-1 relative orbits, demonstrating enhanced temporal resolution and improved runoff onset estimate agreement with snow pillow reference measurements across 10 stratovolcanoes in the Pacific Northwest of the United States (Gagliano et al., 2023). Here, we refine and scale this approach globally, combining our multi-orbit methodology – which provides multiple independent observations across different viewing geometries and times – with a custom MODIS-derived snow phenology dataset to constrain the temporal search window for runoff onset estimation. This integrated approach addresses several key challenges in snowmelt runoff onset detection, including many of those identified by Carletti et al. (2025): coarse temporal resolution of individual relative orbits, sensitivity to viewing geometry, false detection from isolated melt episodes, and false detection in locations or time periods where no seasonal snow exists.

Using this refined methodology, we present a global dataset of snowmelt runoff onset timing for 2015-2024. We document the data processing workflow, describe the dataset structure, validate the dataset against a network of automated weather stations, establish empirically-derived usage recommendations, and discuss key characteristics and limitations. This dataset provides unprecedented global coverage of snowmelt timing at high spatial resolution, offering valuable information for hydrological modeling, water resource management, and ecological research.

https://doi.org/10.5194/essd-2026-216
Preprint. Discussion started: 28 April 2026

Open Access Earth System Science Data Discussions

2 Data and methods

2.1 Input data sources

2.1.1 Sentinel-1 SAR backscatter

We utilized the entire archive of Sentinel-1 C-band SAR data in Interferometric Wide mode, available as radiometrically terrain-corrected (RTC) Cloud-Optimized GeoTIFF files hosted on Microsoft Planetary Computer (Microsoft Open Source et al., 2022). For each water year from 2015 to 2024, we selected all available VV-polarized scenes, which have demonstrated superior performance for snowmelt runoff onset identification when compared to VH polarization (Darychuk et al., 2023). Though the RTC images are available at 10-meter resolution, we leveraged the pre-computed 80-meter overview embedded in the Cloud-Optimized GeoTIFF files in order to balance computation costs, accuracy, and spatial resolution. This resolution selection aligns with Manickam and Barros (2020), who found through area-variance scaling analysis that SAR backscatter measurements of snow exhibit minimum variance at characteristic spatial scales (~100-1000 m depending on terrain and forest cover), suggesting that our 80 m resolution captures wet snow spatial variability while remaining computationally efficient.

2.1.2 MODIS snow cover

We used the 500-meter resolution MODIS MOD10A2 8-day maximum snow extent product (Hall & Riggs, 2021) hosted on Microsoft Planetary Computer (Microsoft Open Source et al., 2022) to prepare a custom snow phenology dataset. This product accounts for cloud cover by reporting the maximum snow extent from up to eight daily observations, recording snow presence if detected on at least one cloud-free day within each eight-day period.

2.1.3 Automated weather station network

For in situ estimation of snowmelt runoff onset, we accessed snow pillow measurements in the Western U.S. from both the SNOTEL network (Fleming et al., 2023; USDA Natural Resources Conservation Service, 2022) and the network operated by the California Cooperative Snow Surveys program, available through the California Data Exchange Center (California Department of Water Resources, 2025). To improve SNOTEL site geolocation accuracy, we used updated coordinates for 455 SNOTEL site locations (Detre et al., 2025). Though the snow pillow data are available with an hourly interval, we used daily values because they are quality-controlled and reduce measurement noise (Fleming et al., 2023).

2.1.4 Forest cover fraction

We used the forest cover fraction layer from the Copernicus Global Land Service PROBA-V land cover dataset (Buchhorn et al., 2020) to characterize how forest cover influences runoff onset detection. This global product is derived from PROBA-V

https://doi.org/10.5194/essd-2026-216
Preprint. Discussion started: 28 April 2026

Open Access Earth System Science Data Discussions

satellite observations and ancillary datasets, and includes fractional land cover layers representing the percentage ground cover of 10 different land cover classes at 100-meter resolution.

2.2 Dataset creation methodology

We developed a workflow that integrates two complementary remote sensing datasets to detect snowmelt runoff onset reliably at a global scale (Fig. 1). First, we created a custom MODIS-derived snow phenology dataset to identify where and when seasonal snow exists. Within these constraints, we analyze Sentinel-1 SAR backscatter time series to detect characteristic minima that indicate runoff onset. This approach leverages the individual strengths of both sensors: MODIS provides reliable snow cover detection and timing constraints that Sentinel-1 cannot achieve alone, while Sentinel-1 offers superior spatial resolution, weather-independent observations, and sensitivity to liquid water content changes during snowmelt. To create the global snowmelt runoff onset dataset, we scaled this methodology using a distributed computing architecture that processed over 100 TB of Sentinel-1 data acquired between 2014-10-01 and 2025-03-31.

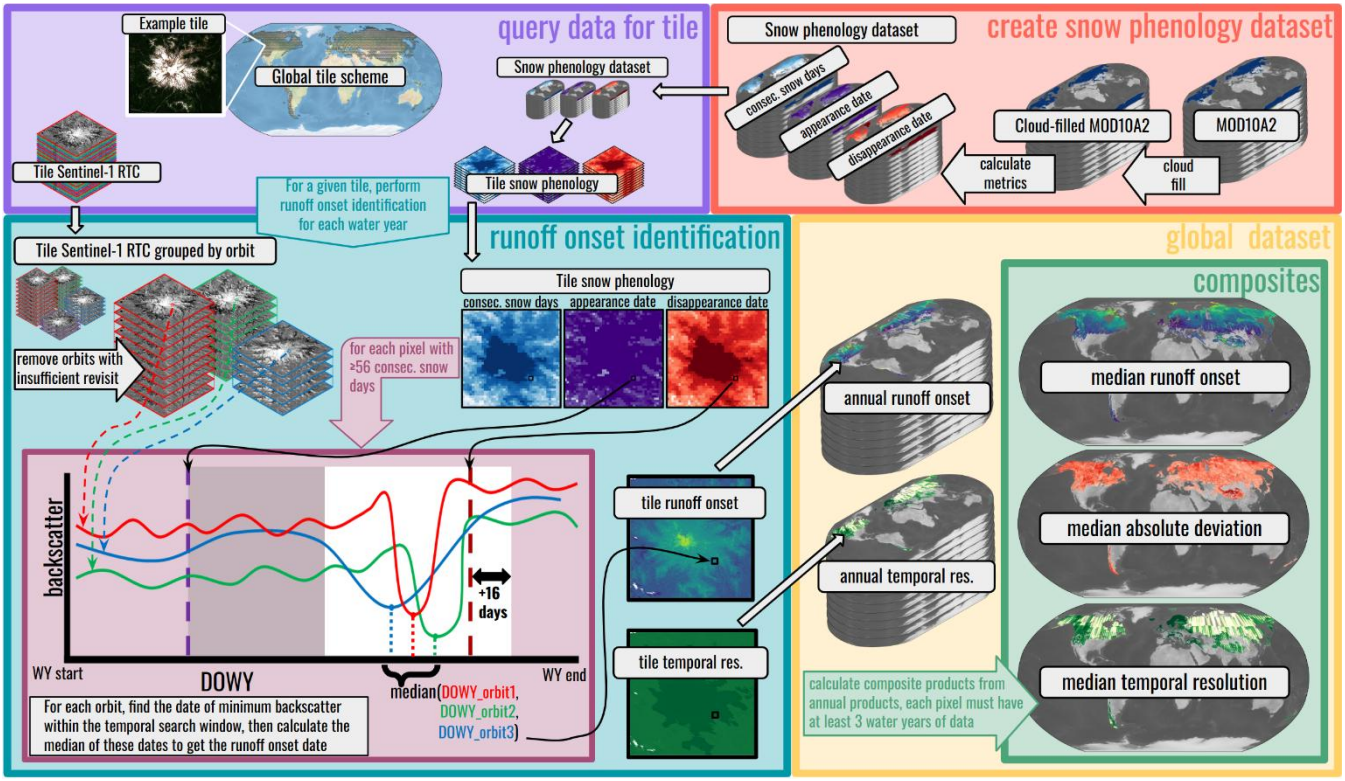

Figure 1. Graphical representation of the workflow used to create the global snowmelt runoff onset dataset. The MODIS-derived snow phenology dataset is initially created (top right) to guide runoff onset identification. For a given processing tile (example shows Mt. Rainier, WA), the Sentinel-1 RTC backscatter data and snow phenology dataset are both subset for all water years (top left). To calculate runoff onset for a single water year (center left), Sentinel-1 data are first grouped by relative orbit and filtered to ensure sufficient revisit interval. For every pixel with ≥ 56 consecutive snow days in the snow phenology dataset, the backscatter minimum within the temporal search window (spanning from the midpoint of the snow-covered period through 16 days after the snow disappearance date, illustrated as a

https://doi.org/10.5194/essd-2026-216
Preprint. Discussion started: 28 April 2026

white background) is identified across multiple relative orbits and the median date becomes the runoff onset estimate (bottom left inset). The resulting products for the tile are mosaicked to create global annual products (center right), and global composite products are created from the stack of annual products (bottom right).

2.2.1 Snow phenology dataset

Central to our methodology was the development of a custom MODIS-derived snow phenology dataset (Gagliano, 2025b) generated from the MODIS MOD10A2 8-day maximum snow extent product using the MODIS_seasonal_snow_mask software library (Gagliano, 2025c). Snow phenology refers to the seasonal timing of snow cover events, including snow appearance, persistence, and disappearance patterns (Tang et al., 2022). This snow phenology dataset provides the foundational spatial and temporal constraints for the runoff onset workflow by defining where (using the snow cover product) and when (using the snow appearance and snow disappearance date products) to search for runoff onset signals in the Sentinel-1 data for each water year.

The MOD10A2 8-day maximum snow extent product represents the maximum snow extent observed over each 8-day MODIS compositing period, which reduces cloud contamination compared to daily observations, yet still contains substantial data gaps due to clouds and polar darkness that obscure snow presence during critical transition periods. We applied an enhanced cloud-filling algorithm that builds on the methodology of Wrzesien et al. (2019), which assumes that snow-covered observations bracketing cloudy periods indicate continuous snow presence – an assumption that is particularly useful during the persistent cloud cover that coincides with the spring snowmelt season. This algorithm operates continuously across all years before water year segmentation, ensuring proper capture of continuous snow periods spanning water year boundaries. For polar regions above ~70° latitude, we implemented additional filtering to remove false “no snow” classifications during polar night periods, when the ~10:30 AM local MODIS observations are unreliable due to darkness.

We extracted three key variables for each pixel and water year from these cloud-filled time series: the number of continuous snow cover days, snow appearance date (first date of continuous snow cover), and snow disappearance date (first day after the last date of continuous snow cover). For pixels with multiple snow-covered periods within a single water year, we selected the longest continuous period.

These variables constitute valuable snow phenology data for the broader scientific community – beyond serving as a fundamental input dataset for our runoff onset methodology, this 10-year global snow phenology dataset offers globally consistent characterization of high-priority observables (snow cover, snow appearance date, and snow disappearance date) that can inform water resource management, ecological studies, and climate change research (Gagliano, 2025b).

2.2.2 Snowmelt runoff onset identification

We limited identification of snowmelt runoff onset to pixels identified with seasonal snow cover for the respective water year in our snow phenology dataset. Specifically, we analyzed pixels with at least 56 days of continuous snow presence, approximating the 60-day threshold from Sturm et al. (1995) with the 8-day temporal resolution of our phenology product. This threshold serves two purposes: it excludes ephemeral snow events with minimal hydrological impact, and it ensures

https://doi.org/10.5194/essd-2026-216
Preprint. Discussion started: 28 April 2026

sufficient time for complete snowmelt phase progression (warming, ripening, and runoff), which is necessary for reliable detection of the characteristic backscatter minimum associated with runoff onset (Carletti et al., 2025).

For pixels meeting this seasonal snow presence criterion, we analyzed the temporal evolution of Sentinel-1 VV-polarized backscatter to identify snowmelt runoff onset. Our preprocessing workflow included quality filtering to remove unrealistically low backscatter values (VV backscatter < -30 dB) and border noise artifacts (Ali et al., 2018), followed by temporal filtering using our snow phenology dataset to restrict analysis to the appropriate temporal detection window for each pixel and water year.

We processed each Sentinel-1 relative orbit independently to account for systematic backscatter differences between viewing geometries caused by varying incidence angle and azimuth orientation. Each relative orbit maintains consistent viewing geometry while providing regular temporal sampling of the same location, typically every 12 days, with overpass times in the early morning for descending relative orbits (~6 AM local) and early evening for ascending relative orbits (~6 PM local). To ensure adequate temporal sampling, we did not consider relative orbits that had any gap exceeding 30 days between consecutive acquisitions within the snow-covered period.

For each valid relative orbit, we identified the timing of minimum backscatter for a given pixel, searching from the midpoint of the snow-covered period through 16 days after the snow disappearance date (two additional 8-day MODIS snow cover periods). We used this constrained temporal search window to reduce the likelihood of false detections from early-season diurnal melt-refreeze cycles and rain-on-snow episodes, which create temporary backscatter minima unrelated to sustained runoff onset. The 16-day extension of the temporal search window accounted for the spatial scale difference between MODIS (500 m) and Sentinel-1 (80 m) data, as residual patches of snow cover may have persisted within the coarser MODIS pixel, even when the MODIS products indicated snow disappearance (Crumley et al., 2020; Pflug et al., 2024).

For each pixel, we calculated the median date across all valid minimum backscatter estimates for available relative orbits to produce a single robust estimate for that pixel and water year. This multi-orbit aggregation approach serves dual purposes: (1) mitigating differences due to viewing geometry and orbit-specific artifacts, and (2) effectively increasing the temporal resolution by combining observations from multiple relative orbits (Gagliano et al., 2023). The resulting annual runoff onset products represent our primary data products within the global snowmelt runoff onset dataset, providing pixel-wise runoff onset timing estimates with global coverage for water years 2015 to 2024. We also estimated the annual average temporal resolution for all pixels with runoff onset timing estimates, calculated by dividing the length of the valid observation window in days by the number of Sentinel-1 observations contained within that period.

We report all runoff onset dates as day of water year (DOWY), with the water year starting on October 1st of the previous year in the northern hemisphere and April 1st of the current year in the southern hemisphere (Aguayo et al., 2021; Cortés & Margulis, 2017).

https://doi.org/10.5194/essd-2026-216
Preprint. Discussion started: 28 April 2026


Open Access Earth System Science Data Discussions

2.2.3 Processing and scaling

The global scope of this analysis, spanning 10 water years across all seasonal snow on Earth, necessitated the development of a scalable, distributed computing approach capable of efficiently processing >100 TB of Sentinel-1 data. To ensure computational feasibility, data integrity, and reproducibility, we implemented an open-source, cloud-based processing architecture.

We partitioned the global domain into 23,520 seamless tiles, each covering 2048 × 2048 pixels (~1.47° × 1.47°, or ~164 × 164 km at the equator). We then pre-allocated a global Zarr data store (Abernathey, 2024) with this global array structure and optimized chunking in order to support parallel processing, where each worker could independently process individual tiles and write results directly to the final data structure without conflicts. This "embarrassingly parallel" approach allowed us to seamlessly scale from small regional processing to full global coverage.

Of the 23,520 total tiles, we limited processing to the 4,453 tiles that contained both seasonal snow and the relevant Sentinel-1 RTC data. Our processing workflow leveraged the Dask computing library, utilizing Dask's lazy evaluation and distributed computing capabilities to coordinate parallel processing across Coiled cloud computing infrastructure (Dask Development Team, 2016). We implemented a multi-stage chunking strategy to optimize memory-bandwidth tradeoffs across distributed workers, applying spatial chunking for I/O-heavy operations to maximize throughput, and temporal chunking for computationally intensive time-series calculations.

We deployed and monitored computing resources in the Microsoft Azure West Europe region, co-located with the relevant Planetary Computer datasets. We predominantly processed tiles in batches of 10, with 60 workers per batch (32 GB memory, 4 cores each), requiring a median of ~4.7 CPU core-hours per tile, totaling ~24,300 CPU core-hours for all tiles.

2.2.4 Generation of 10-year composite products

To aid in the interpretation of the annual snowmelt runoff onset products, we created three additional composite products for pixels with at least three years of valid annual data. We calculated the median snowmelt runoff onset date across all available years, creating a 10-year median snowmelt runoff onset composite product. To estimate interannual variability, we created a 10-year snowmelt runoff onset median absolute deviation composite product. Finally, we created a 10-year local median temporal resolution composite product to capture the temporal resolution of these composites. These complementary products can be used for detailed study of the characteristic snowmelt runoff onset date and variability for any given pixel in the dataset, providing a better understanding of the influence of fixed geographic controls (i.e., elevation, aspect, latitude) and environmental forcing (i.e., temperature and precipitation) on observed snowmelt runoff onset variability (Gagliano, 2025a, Gagliano et al., in prep).

https://doi.org/10.5194/essd-2026-216
Preprint. Discussion started: 28 April 2026

2.3 Dataset evaluation methodology

We employed a two-stage evaluation approach, comparing our snowmelt runoff onset estimates against independent runoff onset estimates from a distributed network of in situ snow water equivalent (SWE) measurements acquired by snow pillows at 946 automated weather stations across the Western U.S. Throughout this paper, we characterize seasonal snowpack magnitude around the time of runoff onset using the water year maximum SWE – the highest daily value recorded at each station within that water year. For our dataset evaluation, we first characterized how forest cover fraction, SWE, and temporal resolution affect agreement between our runoff onset estimates and snow pillow runoff onset estimates using pixel-level residuals aggregated across all stations and water years, and then used these insights to apply appropriate quality filters for station-level evaluation.

For snow pillow runoff onset estimates, we first applied quality filters to daily SWE time series at each station, removing observations with negative SWE values and physically unrealistic apparent daily change (>20 cm/day, Dawson et al., 2016). Further, we excluded water years with less than 10 cm SWE, less than 60 days of continuous snow cover, or data gaps exceeding 10 days, resulting in a total of 7,916 water years of snow pillow time series across 946 stations. Using the filtered time series, we calculated snow pillow runoff onset as the day when SWE decreased below 95% of the water year maximum (or the day of the last occurrence for seasons with multiple SWE decreases below the 95% threshold). We chose this timing instead of directly selecting the timing of maximum SWE in order to account for SWE decreases due to wind redistribution and/or sublimation, as well as to mitigate scenarios where maximum SWE occurs early in a season and persists but doesn't melt significantly until later in the season (Dingman, 2015; Fassnacht et al., 2014). Figure A1 illustrates the snow pillow runoff onset determination and the SAR backscatter minimum determination for two representative water years at a SNOTEL station, showing how both estimates are obtained under favorable high-SWE conditions and more ambiguous low-SWE conditions.

To characterize how forest cover fraction, SWE, and temporal resolution affect agreement between the runoff onset estimates, we computed pixel-wise residuals between our annual runoff onset products and snow pillow estimates within a 1000-meter radius of each station for each of the 10 years in our dataset. We then binned all pixel-wise residuals across all stations and water years by each pixel's respective forest cover fraction, water year maximum SWE (maximum SWE recorded at the respective snow pillow for that water year), and temporal resolution (the pixel-wise temporal resolution for that water year as recorded in the annual temporal resolution product). We calculated the median of each bin to quantify bias, as well as the median absolute deviation of each bin to quantify the spread of the residuals.

For station-level evaluation, we applied quality filters derived from this analysis (forest cover fraction ≤ 0.5, > 20 cm water year maximum SWE, temporal resolution < 14 days; see Sect. 4.1) in order to extract a representative and robust runoff onset estimate for each station and water year. Specifically, for each station and water year, we extracted the median runoff onset date of valid pixels (forest cover fraction ≤ 0.5, temporal resolution < 14 days) within the 1000-meter radius of

https://doi.org/10.5194/essd-2026-216
Preprint. Discussion started: 28 April 2026

each station, and excluded water years with <10% valid pixel coverage or where water year maximum SWE did not reach 20 cm. This resulted in a total of 4,763 water years with valid runoff onset estimates across 735 stations.

For these water years and stations, we computed the timing difference between this representative runoff onset estimate from our annual runoff onset products and the snow pillow runoff onset estimate. To characterize the runoff onset estimate agreement for each water year across all stations, we quantified the bias and spread of the timing differences by computing the median and the median absolute deviation of the residuals.

3 Dataset description

3.1 Dataset overview

The global snowmelt runoff onset dataset contains five groups of products organized in a cloud-optimized Zarr store designed for efficient distributed access, processing, and analysis. The dataset spans the global domain from 180°W to 180°E longitude and 60°S to 81.1°N latitude, encompassing almost all seasonal snow on Earth. All products are provided in geographic coordinates (decimal degrees), using the WGS84 ellipsoid as the horizontal coordinate reference system (EPSG:4326). Pixel spacing is approximately 7.2×10^{-4} degrees, corresponding to 80 meters at the equator. Although longitudinal ground distance per pixel decreases at higher latitudes (e.g., ~40 m at 60°N), the effective spatial resolution of the dataset remains 80 meters across all latitudes because the 80-meter Sentinel-1 RTC overviews were used as input (Sect. 2.1.1). The temporal dimension spans 10 water years (2015-2024), resulting in a complete dataset structure with dimensions (water_year: 10, latitude: 195970, longitude: 499998) for annual products, and (latitude: 195970, longitude: 499998) for the 10-year composite products. Though the original values are integer or floating point numbers, all values are stored as signed 16-bit integers with relevant scaling and offset parameters stored in the metadata, with no-data values of -9999.

3.2 Dataset variables

3.2.1 Annual runoff onset products

The “runoff_onset” variable contains integer day of water year (DOWY) representing runoff onset date estimates for each individual water year from 2015 to 2024, stored as a 3-dimensional array with dimensions (water_year, latitude, longitude). All DOWY dates are relative to their respective hemispheres’ start of water year, discussed further in Sect. 2.2.2. Valid DOWY values range from 1 to 366.

3.2.2 Annual local temporal resolution products

The dataset also includes an accompanying “temporal_resolution” variable to document the average local temporal resolution of the dataset at each pixel for each individual water year (water_year, latitude, longitude). These “temporal_resolution” values are in units of decimal days, with a precision of 0.1 days.

https://doi.org/10.5194/essd-2026-216
Preprint. Discussion started: 28 April 2026


Open Access Earth System Science Data Discussions

3.2.3 10-year composite products

The “runoff_onset_median” variable stores the 10-year median runoff onset composite integer DOWY values (Fig. 2a, Fig. 3), while the “runoff_onset_mad” variable contains the 10-year median absolute deviation composite values in decimal days, with a precision of 0.1 days (Fig. 2b). The “temporal_resolution_median” variable stores the 10-year local median temporal
300 resolution composite values in decimal days, with a precision of 0.1 days (Fig. 2c). These 2-dimensional (latitude, longitude) products are useful for understanding typical runoff onset timing, interannual variability of runoff onset timing, and the typical local temporal resolution of the dataset, respectively. As described in Sect. 2.2.4, these composite products are only calculated at pixels that have 3 or more water years of valid data.

https://doi.org/10.5194/essd-2026-216
Preprint. Discussion started: 28 April 2026

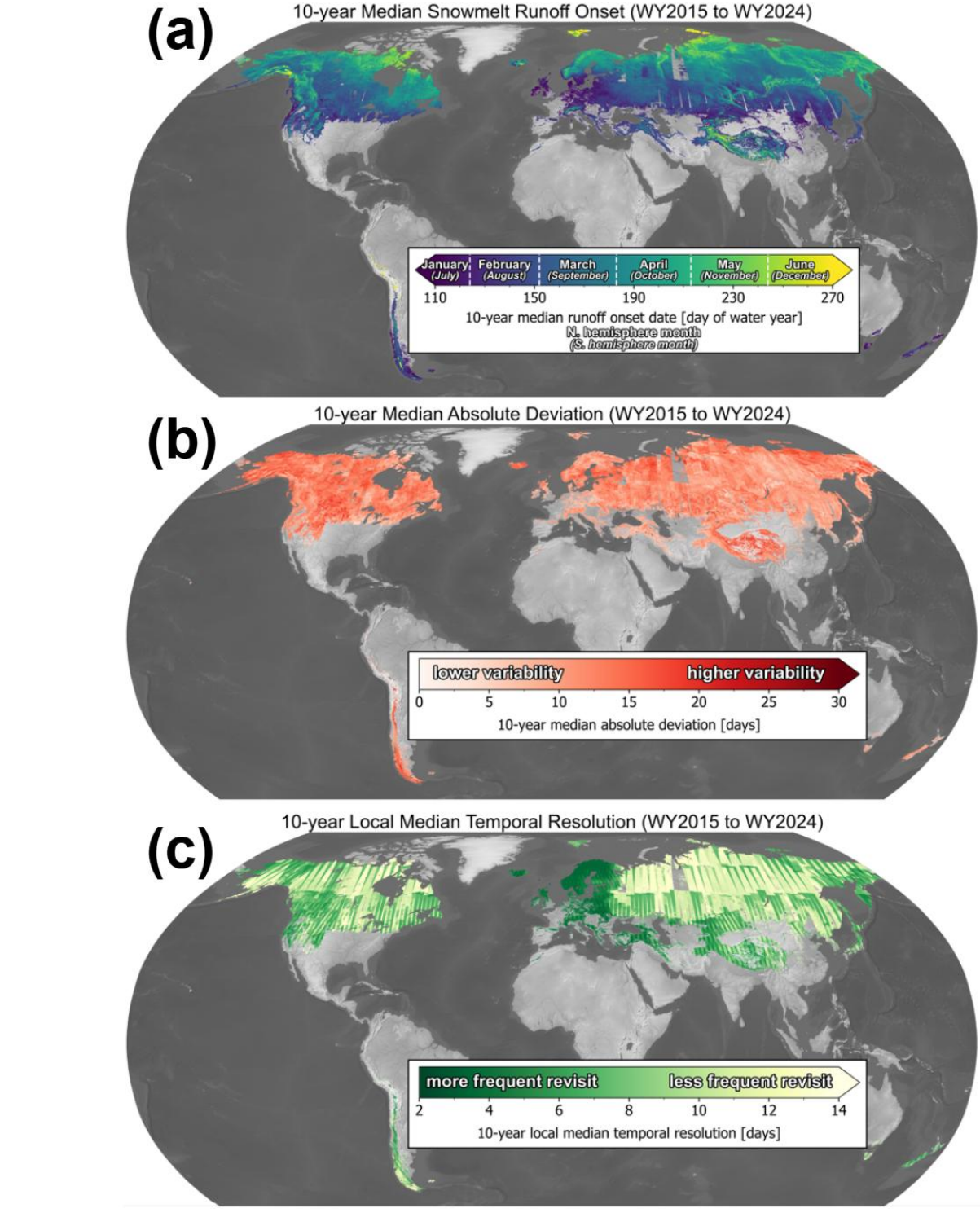

305 **Figure 2.** Global snowmelt runoff onset composite products. **(a)** 10-year median snowmelt runoff onset, **(b)** 10-year median absolute deviation, and **(c)** 10-year local median temporal resolution.

https://doi.org/10.5194/essd-2026-216
Preprint. Discussion started: 28 April 2026

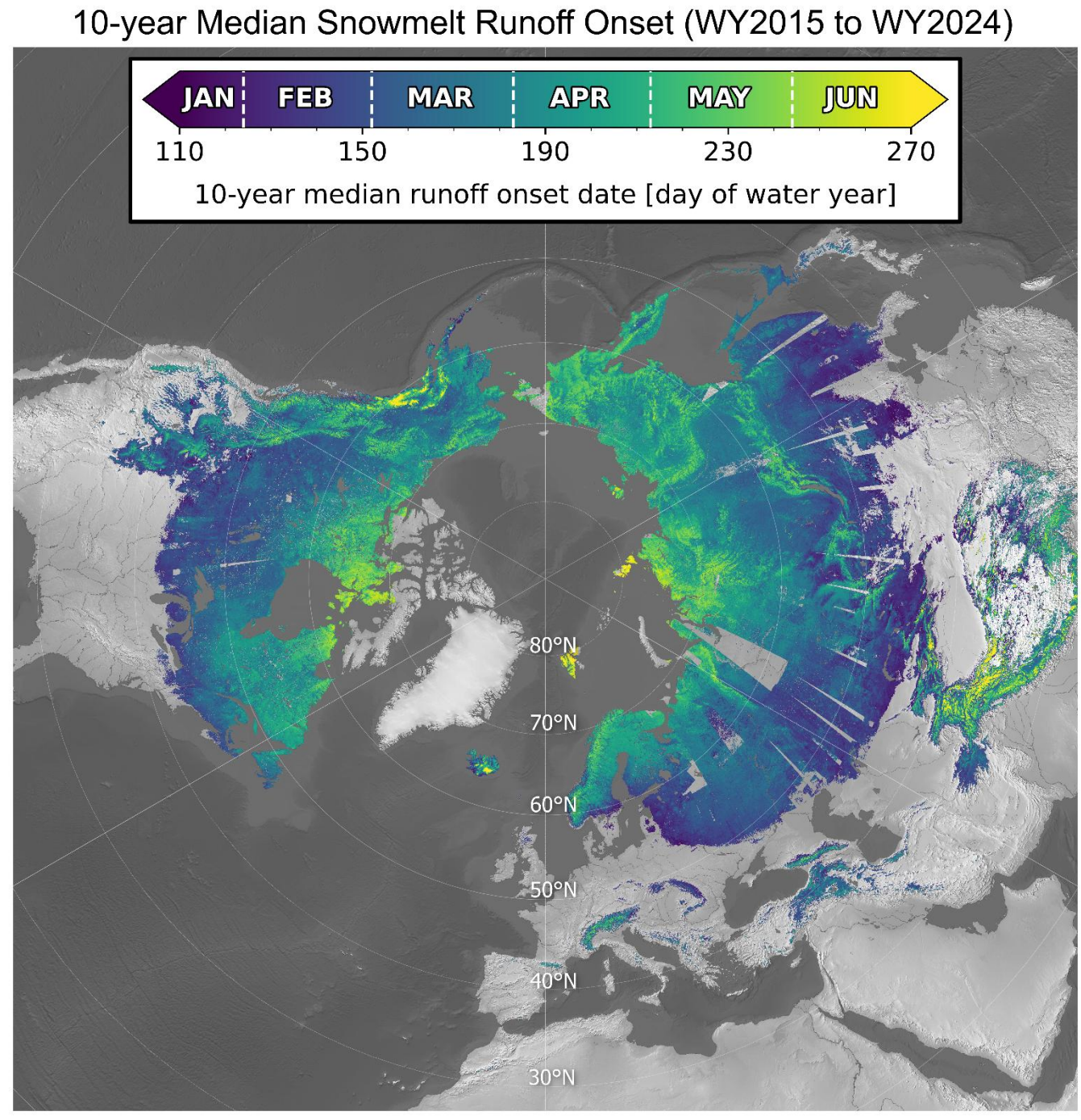

Figure 3. Polar stereographic projection of 10-year median snowmelt runoff onset date for the Northern Hemisphere. See Fig. A2 for polar stereographic maps of all three composite products.

https://doi.org/10.5194/essd-2026-216
Preprint. Discussion started: 28 April 2026

3.3 Spatial coverage and temporal resolution

The spatial coverage of our global snowmelt runoff onset dataset is constrained by the availability of Sentinel-1 Interferometric Wide mode data. Sentinel-1 acquires data over Antarctica and much of the Arctic in Extra Wide mode, so our dataset does not include ~1.6 million km^2 of seasonal snow over the ice-free areas of Greenland, the Canadian Arctic Archipelago, and the Russian Arctic Islands (Liston & Sturm, 2021).

The spatial coverage and temporal resolution of our dataset vary by region and water year (Table 1, Fig. A3, Fig. A4). There are three distinct phases of temporal resolution, largely controlled by the number of active satellites in the Sentinel-1 constellation. Water years 2015 and 2016 have the smallest spatial coverage (8.7-9.8 million km^2, 24-28% of observable seasonal snow extent) and coarsest average temporal resolution (18.2 days). Water years 2017-2021 have expanded spatial coverage (31.6-35.5 million km^2, 87-94% of observable seasonal snow extent) and improved temporal resolution (8.2-9.5 days). Water years 2022-2024 have intermediate spatial coverage (15.7-17.5 million km^2, 44-48% of observable seasonal snow extent) and temporal resolution (8.7-10.9 days).

Across all water years, the overall area-averaged global temporal resolution was 9.2 days, with the 10-year median runoff onset composite covering 36.8 million km^2 (94% of observable seasonal snow extent). Fig. A4 shows the number of water years with valid runoff onset estimates used to prepare the 10-year composites.

Table 1. Global snowmelt runoff onset dataset spatial coverage, observable seasonal snow extent, percent coverage of observable seasonal snow, and average temporal resolution for each water year and the 10-year composites. Spatial coverage represents the total area with valid runoff onset estimates. Observable seasonal snow extent is the annual seasonal snow extent from the MODIS-derived snow phenology dataset, excluding regions without Sentinel-1 Interferometric Wide mode coverage (i.e., Antarctica, Greenland, the Canadian Arctic Archipelago, and Russian Arctic Islands). See Fig. A3 for annual maps of coverage and temporal resolution.

Water year	Spatial coverage [km^2]	Observable seasonal snow extent [km^2]	Coverage [%]	Average temporal resolution [days]
2015	9,779,036	35,396,533	27.6%	18.2
2016	8,690,212	35,762,382	24.3%	18.2
2017	35,539,625	37,692,052	94.3%	9.4
2018	31,639,543	35,897,171	88.1%	9.5
2019	31,818,050	36,517,665	87.1%	8.8
2020	32,028,753	35,992,499	89.0%	9.0
2021	32,430,436	36,003,900	90.1%	8.2

https://doi.org/10.5194/essd-2026-216
Preprint. Discussion started: 28 April 2026

2022	16,006,632	36,317,451	44.1%	9.8
2023	17,542,407	36,634,902	47.9%	8.7
2024	15,702,889	36,043,745	43.6%	10.9
10-year composites	36,761,636	39,200,214	93.8%	9.2

Regional variations in temporal resolution are pronounced across the global domain (Fig. 2c). The finest 10-year median temporal resolution was observed over mainland Europe, with median temporal resolution of 4 days or finer, improving to 2 days or finer in northern Europe. In contrast, the coarsest temporal resolution is observed in northwest North America and northern Asia, with 10-year median temporal resolution of around 12 days. Most other regions fall between these extremes, with 10-year median temporal resolution typically ranging from 6-10 days (Fig. 2c). The temporal resolution varies not only by region, but also locally within regions, reflecting both Sentinel-1 data availability and our pixel-wise processing methodology.

In addition to the 10-year median temporal resolution (Fig. 2c), it is important to consider the spatial variability in the total number of years with valid observations (Fig. A4). Despite coarser temporal resolution, northwest North America has 10 years of valid runoff onset observations, which is similar to northern Europe, while large swaths of northern Asia only have 3-4 years of valid observations.

4 Dataset evaluation

4.1 Effects of forest cover fraction, SWE, and temporal resolution

The pixel-wise analysis reveals that forest cover fraction, SWE, and temporal resolution systematically affect the bias (median) and spread (median absolute deviation) of residuals between runoff onset estimates from our annual products and the in situ snow pillow sensors (Fig. 4).

Forest cover fraction emerges as the dominant control on the bias and spread of residuals. Bias increases with increasing forest cover fraction; for areas with forest cover fraction greater than 0.5, our products show runoff onset occurs 5-20 days earlier than corresponding snow pillow estimates, compared to bias of less than 5 days in areas with forest cover fraction less than 0.5. The spread of residuals is higher (15-25 days) for forest cover fraction greater than 0.5, compared to 5-15 days for forest cover fraction below 0.5.

SWE also influences the bias and spread of residuals, with better agreement in areas with higher observed water year maximum SWE. Bias and spread decrease markedly above approximately 20-30 cm SWE for forest cover fraction below 0.5, with this apparent SWE threshold increasing with forest cover fraction. For forest cover fraction below 0.5 and

https://doi.org/10.5194/essd-2026-216
Preprint. Discussion started: 28 April 2026


Open Access Earth System Science Data Discussions

SWE between 10 and 20 cm, bias approaches 30 days with a spread of up to 21 days, while for SWE between 30 and 40 cm, bias decreases to near 0 and spread is reduced to less than 7 days. Above ~20 cm SWE, residuals continue to decrease with increasing SWE, but with diminishing magnitude.

Increased temporal resolution shows moderate but consistent effects, with both the bias and spread decreasing with improving temporal resolution. This effect is most pronounced between forest cover fraction of 0.4 and 0.7, with spread improving from 21 days for pixels with >14 day temporal resolution, to 14 days for pixels with 7-14 day temporal resolution. This relationship holds for forest cover fraction below 0.4, albeit weaker in strength.

Based on these empirical results, we applied quality filters for the station-level analysis that follows, restricting analysis to pixels with a forest cover fraction below 0.5 and temporal resolution below 14 days, and, at the station level, water years with a maximum SWE greater than 20 cm.

https://doi.org/10.5194/essd-2026-216
Preprint. Discussion started: 28 April 2026

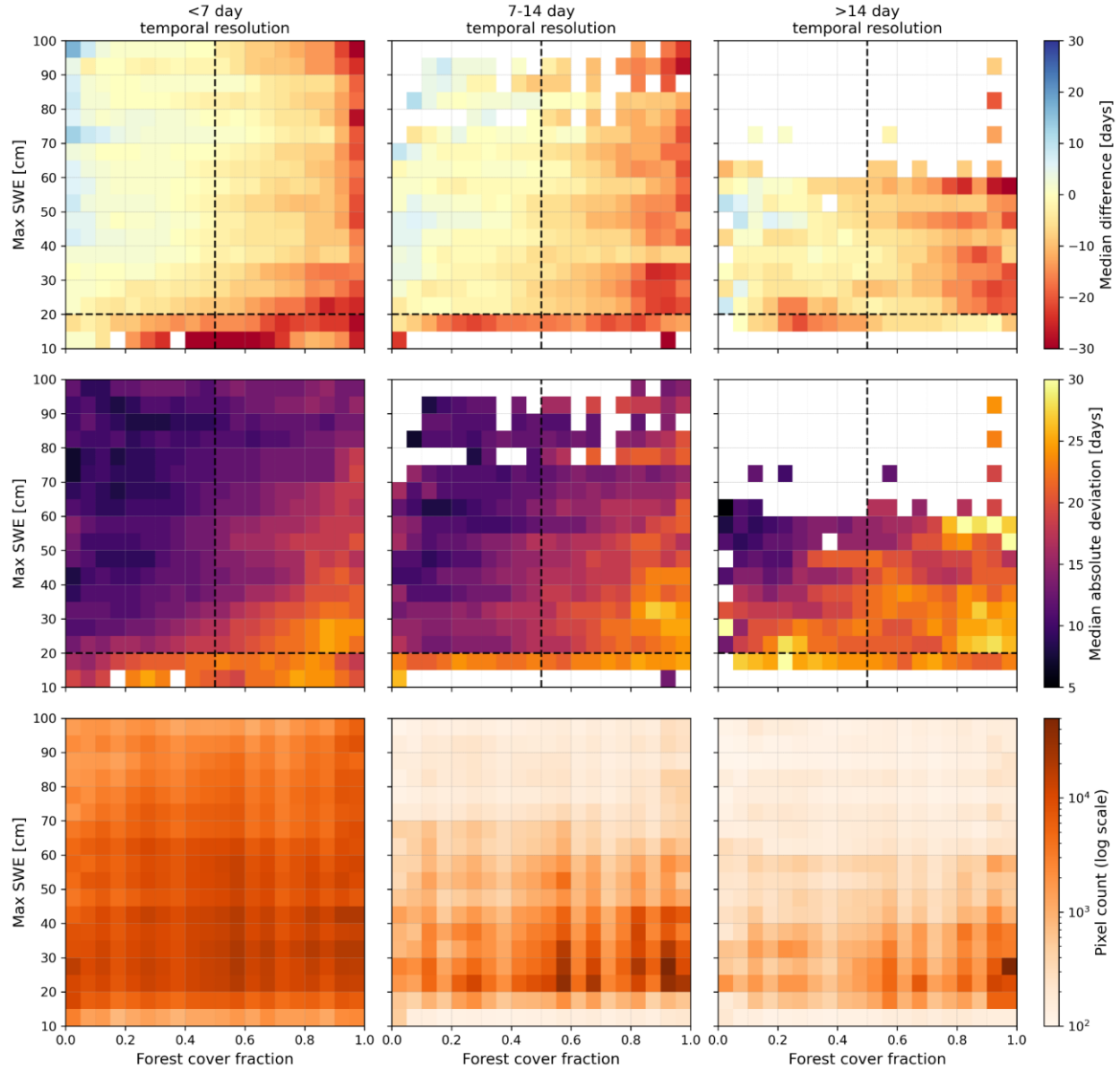

Figure 4. Agreement between our runoff onset estimates and snow pillow runoff onset estimates as a function of forest cover fraction, SWE, and temporal resolution. Top row shows the median of residuals (our product minus snow pillow, used to assess bias), middle row shows median absolute deviation of residuals (used to assess spread), and bottom row shows pixel counts per bin. Metrics are binned for different combinations of forest cover fraction (x-axis), water year maximum SWE (y-axis), and temporal resolution (columns: <7 days, 7-14 days, >14 days). Note increase in the median and median absolute deviation values for forest cover fraction values above 0.5 (vertical dashed lines), water year maximum SWE values less than 20 cm (horizontal dashed lines), and temporal resolution coarser than 14 days (third column).

https://doi.org/10.5194/essd-2026-216
Preprint. Discussion started: 28 April 2026


Open Access Earth System Science Data Discussions

4.2 Automated weather station evaluation results

375 The evaluation of runoff onset estimates from our annual products and the in situ snow pillow sensors revealed generally good agreement with notable temporal and spatial patterns across the Western U.S. (Fig. 5). Across all water years, the bias, represented by the median residual (our product minus snow pillow), was -1.0 days and the spread, represented by the median absolute deviation of residuals, was 9.0 days. In other words, 50% of the runoff onset residuals were within 9 days, which is similar to the dataset temporal resolution for Western North America (Fig. 2c).

380 The spread of residuals varied over the study period (Fig. 5b), though bias remained relatively low in all years. Early years (2015 and 2016) with coarser temporal resolution (9.9-10.6 days for the evaluated stations, compared to the ~18-day global average in Table 1) exhibited a larger spread in residuals (MAD in Fig. 5b). The spread of residuals decreased with finer temporal resolution (4.1-5.6 days) through water years 2017 to 2021. From water year 2022 onward, the average temporal resolution at the stations was 7.3-7.9 days, with a similar spread of residuals.

385 The spatial distribution of residual bias revealed distinct regional patterns (Fig. 5c). Stations with the largest bias, where runoff onset estimates from our annual products occurred up to 30 days earlier than the snow pillow estimates, were concentrated in the southern Rocky Mountains east of the continental divide, where greater forest cover fraction coincides with lower SWE. Conversely, stations with smaller bias (< 7 days) were located in regions with lower forest cover fraction and higher SWE, such as the Sierra Nevada, Colorado Plateau, and the southern Rockies west of the continental divide.

https://doi.org/10.5194/essd-2026-216
Preprint. Discussion started: 28 April 2026

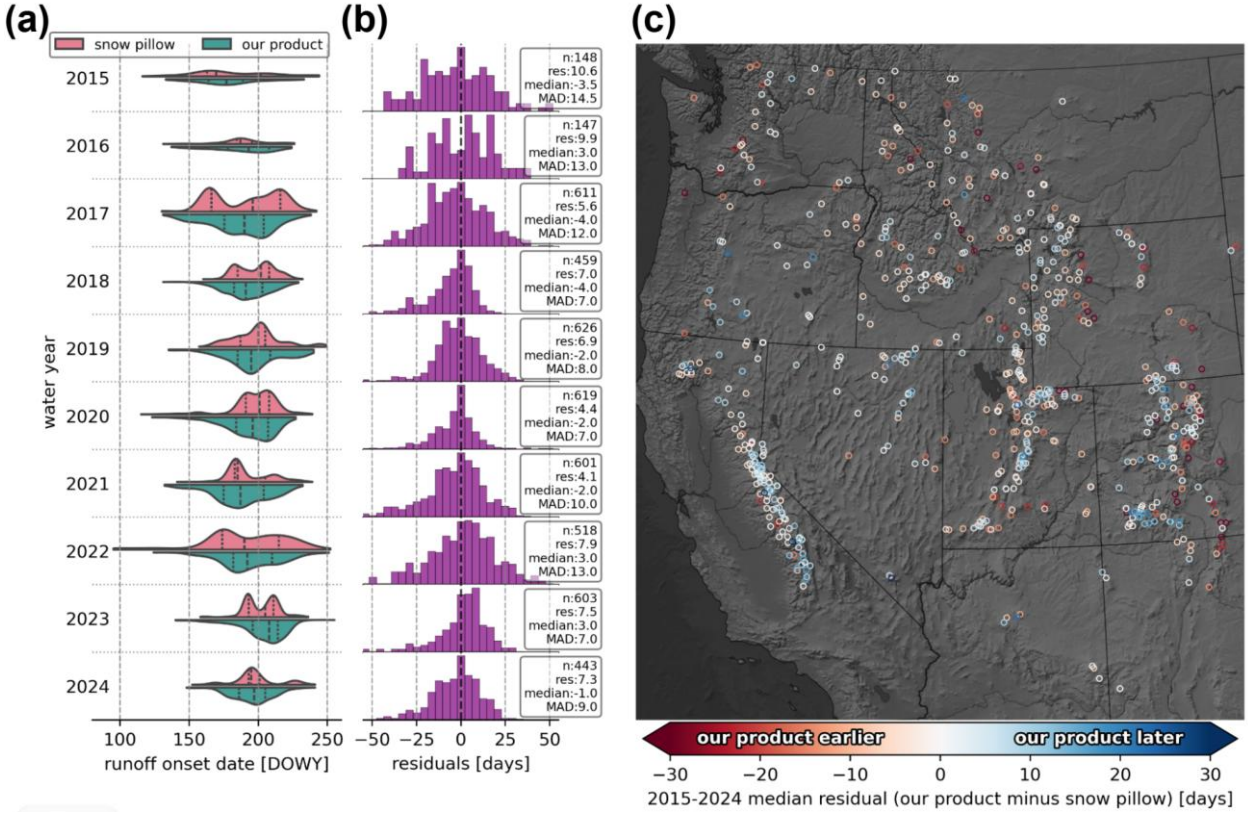

Figure 5. Evaluation of runoff onset estimates from our annual products and 735 automated weather station snow pillow observations for the 10-year period spanning 2015 to 2024. **(a)** Distribution of all directly comparable snowmelt runoff onset estimates for each water year. **(b)** Accompanying histograms of residuals (our product minus snow pillow) for each water year. Text annotations show residual statistics: number of stations (n), average temporal resolution of our annual runoff onset products across evaluated stations (res), median of the residuals (median), and median absolute deviation of the residuals (MAD). **(c)** Median of 2015-2024 residuals (our product minus snow pillow) for each station. At each station, positive values (blue) indicate that the runoff onset estimate from our products usually occurs after the snow pillow estimate, and negative values (red) indicate the runoff onset estimate from our products usually occurs before the snow pillow estimate.

5 Discussion

5.1 Variations in spatial and temporal coverage

This global high-resolution snowmelt runoff onset dataset represents a significant advancement in snow hydrology monitoring, providing unprecedented spatial detail and temporal coverage across Earth's seasonal snow-covered regions. With 80-meter resolution, it bridges a critical observation gap between coarse passive microwave products (typically ~25 km) and sparse, point-scale in situ networks (1 station per ~1280 km^2 in mountain regions of the Western U.S.), while offering a consistent, reproducible methodology applied globally over a decade-long record. This resolution improvement is illustrated in Fig. 6, which compares our annual runoff onset product to the enhanced resolution (6.25 km) passive microwave melt onset product from Pan et al. (2021) over the Alaska Range for water year 2020. Our annual runoff onset

https://doi.org/10.5194/essd-2026-216
Preprint. Discussion started: 28 April 2026

products resolve fine-scale snowmelt variability across complex terrain that is not captured by the passive microwave results, even with enhanced resolution.

Though a comprehensive scientific analysis of our global runoff onset dataset is presented in a complementary study, preliminary examination of the annual products reveals coherent geographic patterns consistent with theoretical expectations of snowmelt across diverse snow environments. Across all continents and latitudes, we observe relatively smooth elevation gradients in snowmelt runoff onset timing – the earliest runoff onset occurs at lower elevations, with runoff onset occurring progressively later at higher elevations.

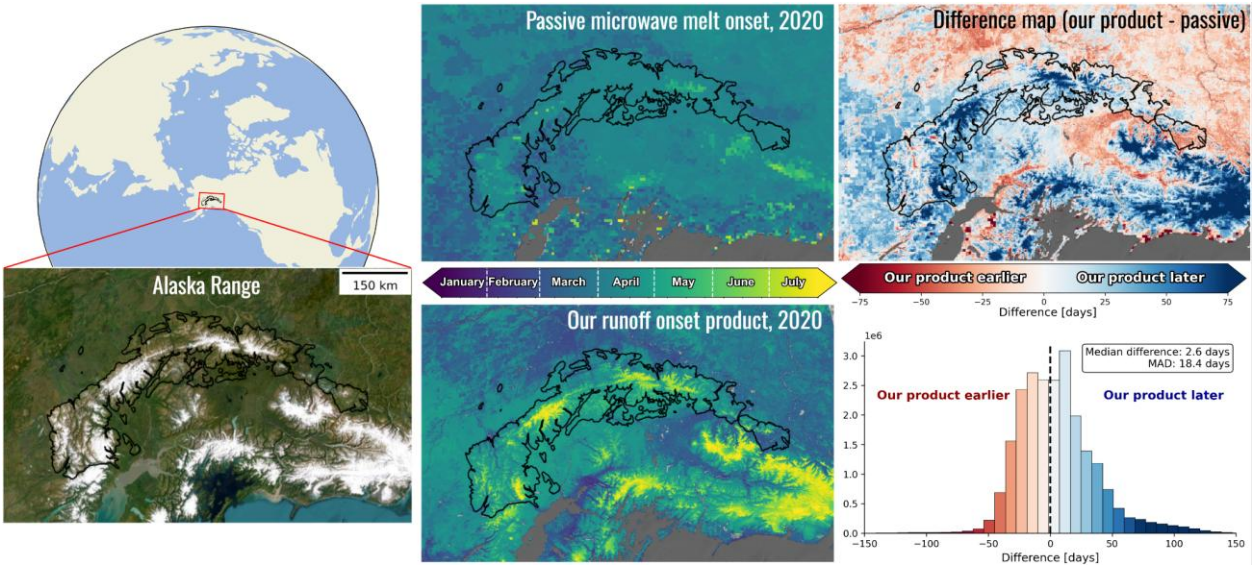

Figure 6. Comparison of snowmelt timing over the Alaska Range for water year 2020 between the ABoVE: Passive Microwave-derived Annual Snowpack Main Melt Onset Date products (Pan et al., 2021) at 6.25 km resolution (top center) and our Sentinel-1 SAR-based annual runoff onset product at 80 m resolution (bottom center). The difference map (top right) and histogram (bottom right) show a median difference of 2.6 days (our product minus passive microwave), with a median absolute deviation of 18.4 days. Despite similar median timing, our runoff onset product reveals spatial heterogeneity that is unresolvable at the passive microwave scale, particularly across complex terrain.

However, dataset spatial coverage and temporal resolution vary systematically across space and time due to the evolving Sentinel-1 constellation and observation plan. The 10-year median temporal resolution composite (Fig. 2c) shows how typical temporal resolution varies from the most frequently observed regions (2-4 days in mainland Europe) to the least frequently observed regions (12+ days in northwest North America and northern Asia). Similarly, dataset spatial coverage and temporal resolution vary by water year, with three distinct temporal phases reflecting the evolving constellation configuration. Water years 2015-2016 represent the early single-satellite period with Sentinel-1A alone, resulting in limited global coverage and coarse temporal resolution. Water years 2017-2021 coincide with the two-satellite constellation following Sentinel-1B's launch in April 2016, enabling more frequent observations that substantially improved spatial coverage and temporal resolution. Water years 2022-2024 reflect single-satellite observations after Sentinel-1B's failure in December 2021, though spatial coverage and temporal resolution remain significantly better than the initial period due to

https://doi.org/10.5194/essd-2026-216
Preprint. Discussion started: 28 April 2026

modifications to the Sentinel-1A observation plan (Potin et al., 2022). As we will detail in the following sections, these variations in temporal resolution introduce spatial variability in the agreement between our runoff onset estimates and snow pillow runoff onset estimates.

5.2 Controls on runoff onset estimate agreement

The three factors identified earlier – forest cover fraction, SWE, and temporal resolution – collectively influence the agreement between our runoff onset estimates and snow pillow runoff onset estimates.

The physical interpretation of SAR backscatter minima can be complex in certain environments, particularly where backscatter change may not be fully attributable to snowmelt dynamics. When pixels contain mixed land cover types – including snow, vegetation, bare ground, structures, or other features – the SAR backscatter may be dominated by non-snow scatterers rather than the snowpack itself, especially for shallow or patchy snow cover. This challenge is most pronounced in forested regions, where C-band SAR represents an integrated response from the forest canopy, the underlying snowpack, and ground surface (Bonnell et al., 2024; Gao & Ma, 2024).

Accordingly, we found that forest cover fraction was the dominant control on runoff onset estimate agreement with snow pillow estimates, with reduced agreement for greater forest cover fraction. This relationship exhibits an approximate inflection point around forest cover fraction of 0.5 (Fig. 4), below which residuals show minimal bias and spread, and above which both bias and spread increase markedly with greater forest cover fraction. Notably, other SAR-based analyses of snow, such as ΔSWE estimation from L-band InSAR (Bonnell et al., 2024) and snow depth estimation from C-band volume scattering (Hoppinen et al., 2024), also observe a degradation in algorithm performance around forest cover fraction of 0.5, suggesting that this value may represent a fundamental physical threshold for SAR penetration through forest canopies to underlying snowpack at ~5-25 cm wavelengths. Above this threshold, the annual runoff onset products indicate runoff onset 5-20 days earlier than snow pillow estimates. This systematic early bias occurs because dense forest canopies fundamentally limit C-band SAR penetration to the underlying snowpack, causing backscatter changes to instead reflect canopy-driven processes including forest disturbance and canopy structural change (Kurum, 2015), tree sway (Raleigh et al., 2022), tree temperature (Bonnell et al., 2024; Lemmetyinen et al., 2022), tree water content (Steele-Dunne et al., 2012), and potentially intercepted snow melting in the canopy (Bonner et al., 2022). Additionally, densely forested areas with warmer winters tend to have frequent winter melt, further complicating runoff onset identification (Lundquist et al., 2013). While forest cover fraction provides a practical means of identifying challenging conditions for our methodology, it remains an imperfect proxy – simple, static forest cover metrics cannot capture the full complexity of SAR interactions with time-variable canopy factors such as canopy structure, canopy disturbance, tree species composition, branch density, and vertical canopy heterogeneity.

We found that SWE also represented an important control on runoff onset estimate agreement with snow pillow estimates, with a critical threshold near 20 cm, below which snowmelt runoff onset could not be reliably detected (Sect. 4.1). While the snow pillow instrument measurement accuracy and precision may also degrade below ~20 cm of SWE when no

https://doi.org/10.5194/essd-2026-216
Preprint. Discussion started: 28 April 2026

longer thermally insulated by overlying snowpack (Johnson & Schaefer, 2002), the observed degradation in runoff onset estimate agreement for less than ~20 cm of SWE reflects the physical limits of C-band SAR detection.

The physical mechanisms underlying this apparent SWE threshold are complex. Fundamentally, detection of snowmelt runoff onset depends on whether the associated characteristic backscatter minimum can be distinguished from the background backscatter variability: that is, whether the backscatter drop during runoff onset exceeds the background dry-snow backscatter variability (i.e., whether the signal-to-noise ratio is sufficient for detection). The underlying ground surface properties, particularly soil moisture and surface roughness, serve as the primary backscatter source when a snowpack is dry (Mätzler, 1987; Nagler et al., 2016). Stronger ground surface backscatter during dry-snow conditions results in a more pronounced backscatter minimum when the snowpack transitions to runoff onset, as signal absorption due to meltwater presence reduces the penetration depth, eliminating the backscatter contribution of the ground surface. Deeper snowpacks with greater SWE contribute additional dry-snow backscatter through enhanced volume scattering (Brangers et al., 2024), increasing the dry-snow backscatter and subsequently increasing the backscatter contrast during runoff onset. Additionally, shallower snowpacks with lower SWE have less cold content and experience more frequent melt-refreeze events, complicating identification of runoff onset. Interestingly, limited C-band penetration depth in wet snow suggests that snow beneath the top ~5-10 cm of the snowpack should not directly influence the backscatter response once the surface is wet (Lund et al., 2020; Nagler, 1996). Yet deeper snowpacks consistently show improved snowmelt runoff onset detection (e.g., Fig. A1), indicating that SWE likely serves as a useful proxy for the environmental conditions that influence the identification of the characteristic backscatter minimum. In this context, improved runoff onset estimate agreement with greater SWE likely reflects two compounding effects: degraded runoff onset estimate agreement in shallow snowpacks with low cold content, as well as improved agreement in deeper snowpacks, where enhanced dry-snow volume scattering increases the backscatter contrast at runoff onset. Finally, the observed dependence of the SWE threshold on forest cover fraction also supports this signal-to-noise interpretation: dense forest canopies introduce additional background backscatter variability, requiring progressively more dramatic backscatter decreases during runoff onset to produce a backscatter minimum detectable above background backscatter variability.

Temporal resolution affected agreement between our runoff onset estimates and snow pillow runoff onset estimates as well, with decreased bias and spread in the residuals as observation frequency improved. This relationship suggests that low observation frequency may not capture the characteristic SAR backscatter minimum, especially during rapid snowmelt transitions. Notably, the effect of temporal resolution was most pronounced at forest cover fraction between 0.4 and 0.7, where forest canopy increases background backscatter variability, making observation frequency more critical.

Besides the effect of improved observation frequency, pixels with finer temporal resolution likely benefit from the aggregation of multiple viewing geometries in our methodology, as they tend to have coverage from multiple independent relative orbits. This might explain the reduced spread of residuals observed in the most densely forested areas (forest cover fraction exceeding 0.7) when temporal resolution is finer than 7 days. Different SAR viewing geometries interact with forest canopies and underlying snowpack at varying incidence angles, potentially allowing some geometries to achieve better

https://doi.org/10.5194/essd-2026-216
Preprint. Discussion started: 28 April 2026

penetration through canopy gaps or reduced canopy interference compared to other viewing geometries. In other words, areas with finer temporal resolution, which benefit from both high observation frequency and multiple viewing geometries, have improved runoff onset estimate agreement with snow pillow estimates, even in challenging densely forested environments.

Areas with a combination of high forest cover fraction, low SWE, and coarse temporal resolution represent the most challenging conditions for reliable snowmelt runoff onset detection, often resulting in bias of up to 20 days and spread exceeding 30 days. Conversely, in areas with forest cover fraction below 0.5, greater than 20 cm SWE, and temporal resolution of less than 14 days, runoff onset estimate agreement with snow pillow estimates is optimal, as bias approaches 0 and spread approaches the temporal resolution of the underlying observations. Importantly, even when one of these factors is sub-optimal – such as moderately high forest cover but adequate SWE and finer temporal resolution, or coarse temporal resolution but sparse forest cover and adequate SWE – the runoff onset estimates typically display acceptable agreement with snow pillow estimates with bias of up to 7 days and spread of 7-14 days.

Finally, the controls examined here are not exhaustive, and other factors likely affect runoff onset estimate accuracy and precision, such as terrain complexity, snow grain size evolution, land cover type and change, soil moisture and roughness, and local meteorological conditions.

5.3 Evaluation and comparison challenges

Our comprehensive evaluation using 735 automated weather stations across the Western U.S. demonstrates strong agreement between runoff onset estimates from our annual products and in situ snow pillows. The overall evaluation metrics – a median difference of -1.0 days and a median absolute deviation of 9.0 days (50% of residuals fall within 9.0 days) – indicate minimal systematic bias and a spread that approaches the temporal resolution of the original Sentinel-1 observations.

The spatial distribution of bias between our runoff onset estimates and snow pillow estimates reveals systematic regional patterns that are consistent with our controls analysis. Stations with the largest biases – where our estimates occurred up to 30 days earlier than snow pillow estimates – were concentrated in the southern Rocky Mountains east of the continental divide, where dense forest cover coincides with low SWE. This regional clustering of large bias reflects the compounding effects of high forest cover fraction and low SWE. On the other hand, regions showing minimal bias correspond to sparse forest cover and high SWE, confirming that the annual runoff onset products perform well under the conditions we identified. This evaluation demonstrates that while forest cover fraction, SWE, and temporal resolution do create systematic regional spatial patterns in runoff onset estimate agreement with snow pillow estimates, our empirically-derived thresholds provide effective guidance for optimal usage of our products.

It is important to emphasize that both our product and snowmelt runoff onset estimates from snow pillow measurements detect snowpack-scale processes – when water drains from the snowpack – rather than basin-scale streamflow response. The timing that we report represents meltwater availability for subsurface infiltration and eventually streamflow

https://doi.org/10.5194/essd-2026-216
Preprint. Discussion started: 28 April 2026


Open Access Earth System Science Data Discussions

contribution, not the arrival of water at stream gauges, which can lag by days to weeks depending on basin characteristics (Frisbee et al., 2011; Lowry et al., 2010).

However, the two approaches detect different physical processes related to runoff onset, introducing natural timing offsets that complicate direct comparison. Snow pillows measure mass change in the snowpack and can register SWE reductions from various processes that may precede or follow actual meltwater outflow, while our SAR methodology aims to identify a characteristic backscatter minimum associated with changes to liquid water content and snow surface roughness that accompany the transition to the runoff phase. For example, sublimation and wind redistribution can modify SWE without changing the liquid water content in a snowpack, potentially leading to snow pillows indicating earlier runoff onset than our product. Conversely, diurnal melt-freeze cycles, rain-on-snow events, and isolated warm periods may temporarily increase liquid water content and alter snow surface roughness before continuous runoff begins, potentially leading to our product indicating earlier runoff onset than the snow pillows. Though our methodology attempts to minimize these early false positive runoff onset estimates by restricting the temporal search window to begin at the midpoint of the snow-covered period (Sect. 2.2.2), we cannot guarantee the removal of false positive runoff onset estimates later in the season. Figure A1 illustrates how these challenges are compounded in shallow snowpack conditions, where snow pillow runoff onset timing becomes highly sensitive to small SWE fluctuations near the 95% maximum SWE threshold, and the signal-to-noise ratio of the SAR backscatter minimum is reduced, leading to larger timing offsets between the two methods. These challenges are further complicated by the episodic nature of snowmelt itself – snowpacks often cycle repeatedly between melt phases, potentially leading to multiple discrete instances of runoff onset in a single season (Dingman, 2015; Lund et al., 2022). Despite such dynamic melt seasons, our median aggregation of runoff onset estimates across multiple individual relative orbits provides robustness against such variability. Accordingly, the reported runoff onset dates from our annual runoff onset products are best understood as a robust characterization of the seasonal transition to sustained meltwater release rather than a precise timestamp of a single discrete event.

Beyond these fundamental measurement differences, several methodological constraints introduce additional uncertainty into the evaluation effort. First, the two methods have different temporal sampling: the snow pillow measurements have daily intervals, while the SAR observations occur at intervals ranging from 6 to 24 days depending on the Sentinel-1 observation plan. This difference in temporal sampling manifests in the distribution of runoff onset estimates by water year (Fig. 5a). The bimodal distribution of daily snow pillow estimates reflects the influence of discrete synoptic-scale weather-related melt events in distinct Western U.S. maritime and continental snowmelt timing regimes (Musselman et al., 2021), whereas the coarser and spatially variable temporal resolution of our products yields more normal distributions. Additionally, snow pillow measurement errors, such as meltwater pooling on the instrument surface, can distort the timing of SWE reduction (Webb et al., 2017). Finally, snow pillow and SAR geolocation uncertainty, as well as scale differences between point-based snow pillow measurements and the 80-meter SAR pixels within the 1000-meter station radius, contribute to timing differences in the methods. Local spatial variability in SWE and snowmelt timing around these stations can be substantial over short distances, introducing uncertainty in representativeness (Meromy et al., 2013). However,

https://doi.org/10.5194/essd-2026-216
Preprint. Discussion started: 28 April 2026

statistical aggregation over the 4,763 water years across 735 stations ensures that these local effects do not compromise the overall conclusions of the evaluation.

Despite these challenges, the overall agreement between our runoff onset estimates and snow pillow estimates confirms that our methodology can reliably detect snowmelt runoff onset across diverse landscapes. The observed temporal evolution (Fig. 5b) further suggests that agreement between our runoff onset estimates and snow pillow estimates is primarily constrained by observation frequency rather than fundamental methodological issues.

5.4 Recommendations for dataset users

Though we discuss the physical underpinnings and compound effects of forest cover fraction, SWE, and temporal resolution in Sect. 5.2, here we provide more direct recommendations for users of our dataset.

For optimal usage of our annual runoff onset products, users should limit analysis to areas with forest cover fraction below 0.5, SWE above ~20 cm, and temporal resolution less than 14 days. Under these combined conditions, users can expect near-zero systematic bias and spread approaching the temporal resolution of the underlying observations. When only one factor is sub-optimal, the products typically remain useful, though users should avoid using the products in areas where multiple challenging conditions coincide. Users should consider the local temporal resolution when interpreting runoff onset dates for a given water year (see Fig. A3). In practice, these thresholds are best interpreted as approximate guidelines, as the underlying relationships are complex, and conditions just outside the recommended ranges may still yield useful estimates.

Additionally, in extreme high-elevation regions above 5000 m (~5% of the global seasonal snow area covered by our dataset), particularly in the tropical Andes and parts of High Mountain Asia, sublimation can often surpass snowmelt as the primary snow ablation mechanism (Ayala et al., 2023; Gascoin et al., 2013; Réveillet et al., 2020). The physical interpretation of backscatter minima in sublimation-dominated environments remains poorly understood, so we caution against the use of our snowmelt runoff onset dataset in such locations, especially if site-specific validation is not possible.

Finally, our snow phenology dataset inherits known MODIS snow product limitations, including false positive snow presence identification in a small number of geographic settings – near turbid water bodies (e.g., on the Tibetan Plateau), over salt flats (e.g., in the Atacama Desert), and in regions with near-permanent cloud cover where cloud-snow misclassification is common (primarily the eastern slopes of the tropical Andes) (Hall & Riggs, 2021; Saavedra et al., 2017). These inherited false positive snow presence values can cause our algorithm to search for runoff onset where no snowpack existed, resulting in spurious estimates in the annual runoff onset products. Users with study areas in these specific settings – adjacent to turbid water bodies, over salt flats, or on the eastern slopes of the tropical Andes – are therefore encouraged to consult ancillary land cover data or independent snow cover data to verify snow presence in suspect pixels.

5.5 Applications and future work

This global snowmelt runoff onset dataset enables diverse applications across multiple disciplines. The annual runoff onset timing products can provide critical retrospective information on the location and timing of snowmelt for hydrological

https://doi.org/10.5194/essd-2026-216
Preprint. Discussion started: 28 April 2026

applications. This information can enable the study of the relationship between the spatial distribution of snowpack properties (e.g., snow depth and SWE) and downstream runoff timing and runoff volume. These insights could ultimately inform streamflow forecasting, especially in snow-dominated watersheds and watersheds lacking in situ observations.

We demonstrate the scientific potential of this dataset in a complementary study that examines systematic relationships between geographic, topographic, and climatic factors governing snowmelt timing across diverse mountain environments, providing insights into the fundamental drivers of global snowmelt variability (Gagliano, 2025a, Gagliano et al., in prep). We also consider the global population exposure to snowmelt timing variability through basin-scale evaluation of observed runoff onset timing anomalies across snow-dependent watersheds, revealing potential population vulnerability to interannual variability in runoff onset timing (Gagliano et al., in prep).

Our dataset also offers broader insights into the spatial and temporal variability in snowmelt timing, which represents a sensitive indicator of climate change impacts in mountain environments. As the satellite record continues, researchers can analyze longer-term trends in snowmelt timing, as well as the relationships between snowmelt patterns and improved climate forcing data, potentially revealing teleconnections between large-scale atmospheric patterns and regional snowmelt dynamics. The capability of this dataset to detect anomalously early or late melt timing makes it particularly valuable for examining snowmelt responses to climate anomalies.

More specialized scientific applications include investigating the coupled snow-fire system, where early snowmelt promotes more severe wildfire (Balik et al., 2026), and wildfire in turn modifies subsequent snowmelt timing (MacDonald et al., 2022; Rickenbaugh et al., 2026). Other scientific applications include examining the influence of light-absorbing particles and radiative forcing on spatial patterns of snowmelt timing (Skiles et al., 2018), quantifying the effect of forest properties on snowmelt timing (Lundquist et al., 2013), investigating the effects of forest management on snowmelt timing (Christopher-Moody, 2025), and examining the phenological responses to snowmelt across complex mountain terrain (John et al., 2020; Matias et al., 2024). Beyond these scientific applications, our dataset could enhance snowpack and hydrological model performance in data assimilation systems (Mirza et al., 2025), and can also help define the optimal spatial and temporal windows for reliable snow property retrievals from complementary remote sensing approaches – including Sentinel-1 volume scattering methods for snow depth estimation (Hoppinen et al., 2024; Lievens et al., 2022), and L-band InSAR ΔSWE estimation relevant to the recently launched NISAR mission (Alabi et al., 2025; Bonnell et al., 2021; Kaur et al., in revision; Palomaki & Sproles, 2023; Tarricone et al., 2023).

Future improvements in the temporal and spatial coverage of satellite SAR measurements could enhance the quality and coverage of future datasets created using our methodology. The launch of Sentinel-1C in December 2024 restored the Sentinel-1 constellation to two operational satellites, and Sentinel-1D launched in November 2025. When Sentinel-1D becomes fully operational, it will replace the aging Sentinel-1A, ensuring long-term continuity of the two-satellite configuration. For global snowmelt runoff onset applications, this two-satellite configuration, as demonstrated by the 2017-2021 period in this dataset, yields superior spatial coverage, temporal resolution, and runoff onset estimate agreement with snow pillow estimates relative to single-satellite operations. The recently launched L-band NISAR mission offers potential to

https://doi.org/10.5194/essd-2026-216
Preprint. Discussion started: 28 April 2026

extend snowmelt detection beneath dense forest canopies due to greater penetration through vegetation than the C-band Sentinel-1 data. Though limited by proprietary data policies and spatial coverage, rapidly expanding commercial SAR constellations offer sub-daily revisit capabilities and very high spatial resolution, which could enable even more precise estimation of snowmelt timing. These advances in satellite SAR, combined with continued algorithm refinements and expanded validation efforts across different geographic regions and climate zones, will enhance future dataset versions and broaden their applicability across an even wider range of scientific and applied contexts.

6 Data and code availability

The global snowmelt runoff onset dataset is available at https://doi.org/10.5281/zenodo.16953614 (Version 1.1.0, Gagliano et al., 2026), and the software used to generate it is available at https://github.com/egagli/global_snowmelt_runoff_onset (Gagliano, 2026). The MODIS-derived snow phenology dataset is available at https://doi.org/10.5281/zenodo.15692530 (Gagliano, 2025b), and the software used to generate it is available at https://github.com/egagli/MODIS_seasonal_snow_mask (Gagliano, 2025c).

7 Conclusions

This global snowmelt runoff onset dataset provides the first comprehensive high-resolution characterization of snowmelt timing across Earth's seasonal snow-covered regions. By combining multiple orbital geometries of Sentinel-1 C-band SAR with a custom MODIS-derived snow phenology dataset, we developed a robust methodology for detecting the characteristic backscatter minimum associated with snowmelt runoff onset, producing a global 80-meter snowmelt runoff onset record spanning water years 2015 to 2024.

A comprehensive evaluation of our dataset using 735 automated weather stations in the Western U.S. over a 10-year period confirmed the reliability of our methodology, with a median difference of -1.0 days and a median absolute deviation of 9.0 days compared to in situ snow pillow measurements. We performed a systematic analysis to understand the effects of forest cover fraction, SWE, and temporal resolution on runoff onset estimate agreement with snow pillow estimates. Forest cover fraction emerged as the dominant control, with strong agreement below forest cover fraction of 0.5. We identified a critical threshold of ~20 cm of SWE, below which snowmelt runoff onset could not be reliably detected. Finally, we observed improved agreement with finer temporal resolution.

This open dataset and associated open-source tools can support a wide range of applications in hydrology, climate science, ecology, and water resource management. The methodological framework and empirically-derived usage recommendations provide guidance for appropriate dataset application and may inform future SAR satellite mission requirements for snow observations. Together, this dataset and methodology add to the growing body of observations needed to better understand and monitor global snowmelt in the coming decades.

https://doi.org/10.5194/essd-2026-216
Preprint. Discussion started: 28 April 2026

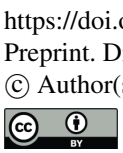

Open Access Earth System Science Data Discussions

Appendix A

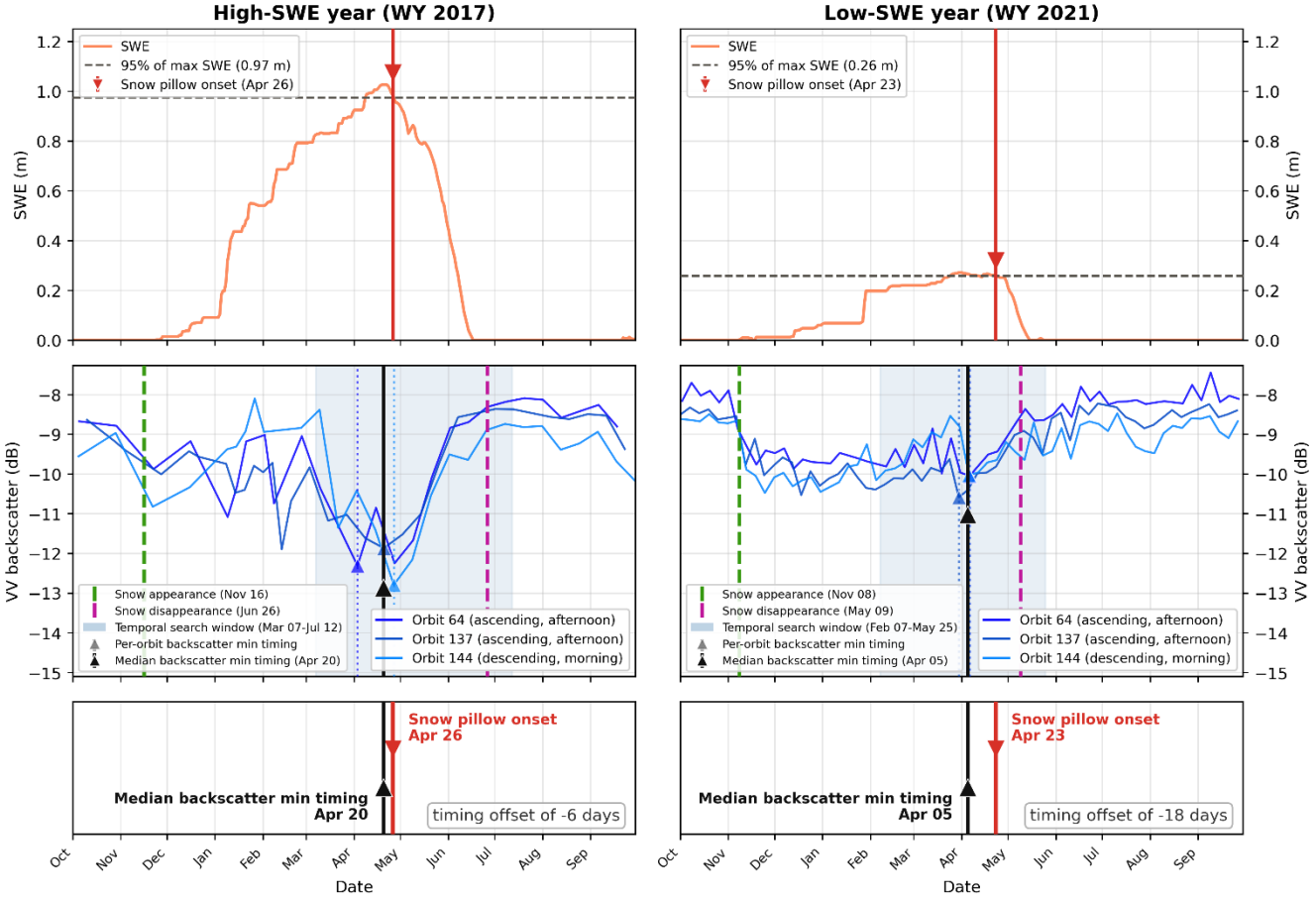

Figure A1. Snow pillow runoff onset and Sentinel-1 SAR backscatter minimum timing at Virginia Lakes Ridge SNOTEL station in California (846_CA_SNTL) for a high-SWE water year (WY 2017, left column) and a low-SWE water year (WY 2021, right column). Top panels show daily in situ snow pillow SWE measurements, horizontal dashed line marks 95% of maximum measured SWE for the water year, and red vertical line with triangle indicates the snow pillow runoff onset date – the day when SWE decreased below the 95% threshold (Sect. 2.3). Middle panels show Sentinel-1 backscatter time series for each relative orbit (blue solid lines). Green and purple dashed vertical lines indicate snow appearance and disappearance dates, respectively, from the MODIS-derived snow phenology dataset. The shaded blue region denotes the temporal search window for the backscatter minima determination (Sect. 2.2.2), dotted vertical lines with colored triangles show the per-orbit timing of backscatter minima, and the bold black vertical line with triangle shows the median timing of the per-orbit backscatter minima – the SAR-derived runoff onset date used for the water year. Bottom panels summarize the signed timing difference between the two runoff onset estimates (SAR minus snow pillow). In the high-SWE year, a well-defined SWE maximum and a pronounced, unambiguous backscatter minimum yield close agreement between methods (-6 days). However, in the low-SWE year, a shallower snowpack leads to a less distinct melt onset signal in both records: SWE near the 95% threshold persists over a broad period, and the backscatter minimum is less pronounced, together introducing ambiguity into both runoff onset estimates and resulting in a larger offset between the two methods (-18 days).

https://doi.org/10.5194/essd-2026-216
Preprint. Discussion started: 28 April 2026

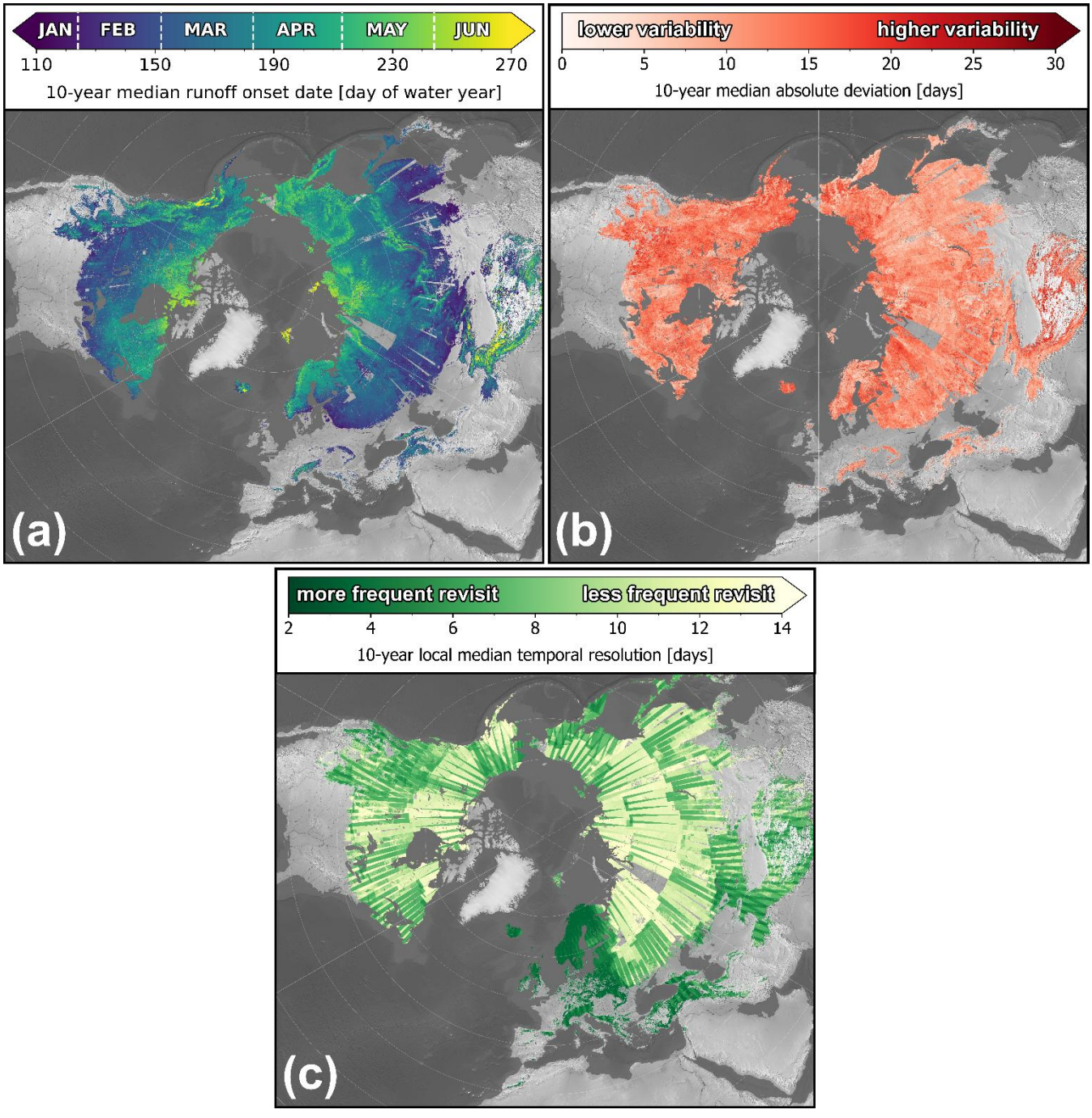

Figure A2. Global snowmelt runoff onset composite products with polar stereographic projection for the Northern Hemisphere. **(a)** 10-year median snowmelt runoff onset, **(b)** 10-year median absolute deviation, and **(c)** 10-year local median temporal resolution composite product.

https://doi.org/10.5194/essd-2026-216
Preprint. Discussion started: 28 April 2026

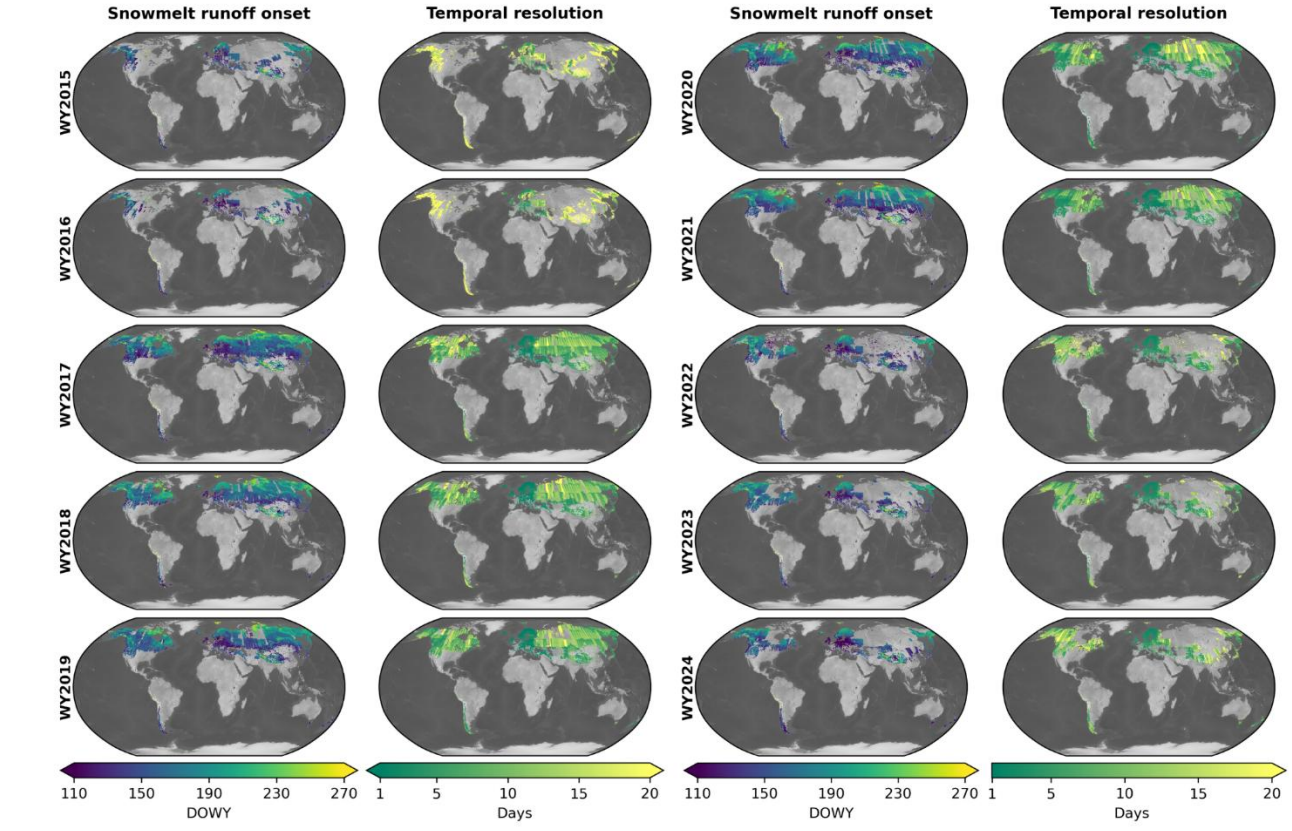

Figure A3. Snowmelt runoff onset (day of water year) and temporal resolution (days) for each water year.

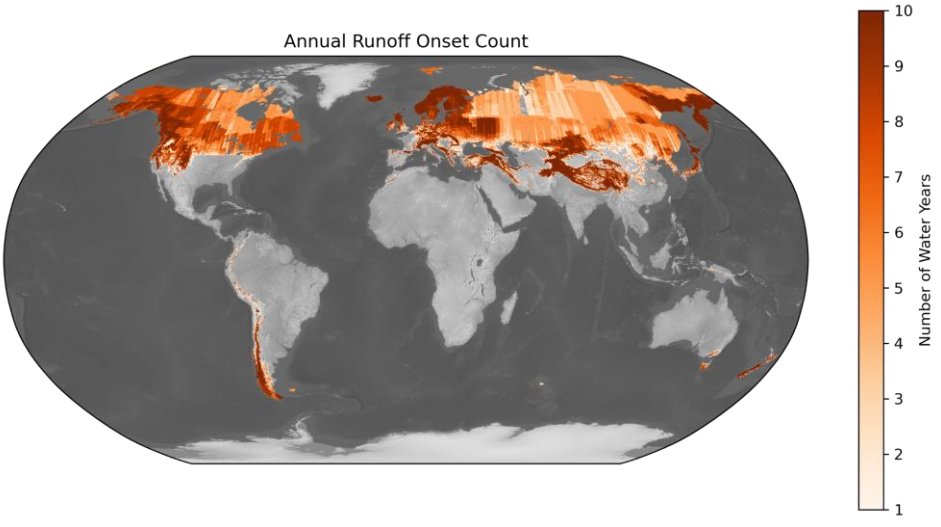

685

Figure A4. Per-pixel count of water years with valid annual snowmelt runoff onset estimates. The variable density of temporal coverage is largely determined by the number of operational satellites in the Sentinel-1 constellation and data acquisition plans.

https://doi.org/10.5194/essd-2026-216
Preprint. Discussion started: 28 April 2026

Author contributions

EG – conceptualization, methodology, data curation, formal analysis, software, manuscript drafting, manuscript review and editing

DS – supervision, project administration, funding acquisition, conceptualization, methodology, resources, manuscript review and editing

SH – project administration, methodology, software, resources, manuscript review and editing

Competing interests

The contact author has declared that none of the authors have any competing interests.

Disclaimer

Copernicus Publications remains neutral with regard to jurisdictional claims made in the text, published maps, institutional affiliations, or any other geographical representation in this paper. While Copernicus Publications makes every effort to include appropriate place names, the final responsibility lies with the authors. Views expressed in the text are those of the authors and do not necessarily reflect the views of the publisher.

Acknowledgements

We would like to thank Lila Rickenbaugh, Mira Khadka, Bareera Mirza, Ally Detre, Preetika Kaur, Marin MacDonald, Kyla Christopher-Moody, and Ross Mower for their feedback on this dataset. We would also like to thank Jessica Lundquist, H.P. Marshall, and Mia Bennett for their insightful comments and subsequent discussions which improved this manuscript.

Financial support

Funding support was provided by U.S. Bureau of Reclamation award R21AC10446, NASA award 80NSSC24K1669, and a NSF Graduate Research Fellowship (DGE-1762114).

References

Abernathey, R. (2024). A Serverless Approach to Building Planetary-Scale EO Datacubes in Zarr. *Earthmover*. https://earthmover.io/blog/serverless-datacube-pipeline/

https://doi.org/10.5194/essd-2026-216
Preprint. Discussion started: 28 April 2026

Aguayo, R., León-Muñoz, J., Garreaud, R., & Montecinos, A. (2021). Hydrological droughts in the southern Andes (40–45°S) from an ensemble experiment using CMIP5 and CMIP6 models. *Scientific Reports*, *11*, 5530. https://doi.org/10.1038/s41598-021-84807-4

Alabi, I. O., Marshall, H.-P., Mead, J., & Trujillo, E. (2025). Advancing terrestrial snow depth monitoring with machine learning and L-band InSAR data: A case study using NASA's SnowEx 2017 data. *Frontiers in Remote Sensing*, *5*, 1481848. https://doi.org/10.3389/frsen.2024.1481848

Ali, I., Cao, S., Naeimi, V., Paulik, C., & Wagner, W. (2018). Methods to Remove the Border Noise From Sentinel-1 Synthetic Aperture Radar Data: Implications and Importance For Time-Series Analysis. *IEEE Journal of Selected Topics in Applied Earth Observations and Remote Sensing*, *11*(3), 777–786. IEEE Journal of Selected Topics in Applied Earth Observations and Remote Sensing. https://doi.org/10.1109/JSTARS.2017.2787650

Awasthi, S., & Varade, D. (2021). Recent advances in the remote sensing of alpine snow: A review. *GIScience & Remote Sensing*, *58*(6), 852–888. https://doi.org/10.1080/15481603.2021.1946938

Ayala, Á., Schauwecker, S., & MacDonell, S. (2023). Spatial distribution and controls of snowmelt runoff in a sublimation-dominated environment in the semiarid Andes of Chile. *Hydrology and Earth System Sciences*, *27*(18), 3463–3484. https://doi.org/10.5194/hess-27-3463-2023

Balik, J., Coop, J., & Parks, S. A. (2026). Snowpack decline kindles more severe fire in the western United States. *Environmental Research Letters*. https://doi.org/10.1088/1748-9326/ae4e4a

Barnett, T. P., Adam, J. C., & Lettenmaier, D. P. (2005). Potential impacts of a warming climate on water availability in snow-dominated regions. *Nature*, *438*(7066), Article 7066. https://doi.org/10.1038/nature04141

Bonnell, R., Elder, K., McGrath, D., Marshall, H. P., Starr, B., Adebisi, N., Palomaki, R. T., & Hoppinen, Z. (2024). L-Band InSAR Snow Water Equivalent Retrieval Uncertainty Increases With Forest Cover Fraction. *Geophysical Research Letters*, *51*(24), e2024GL111708. https://doi.org/10.1029/2024GL111708

Bonnell, R., McGrath, D., Williams, K., Webb, R., Fassnacht, S. R., & Marshall, H.-P. (2021). Spatiotemporal Variations in Liquid Water Content in a Seasonal Snowpack: Implications for Radar Remote Sensing. *Remote Sensing*, *13*(21), Article 21. https://doi.org/10.3390/rs13214223

https://doi.org/10.5194/essd-2026-216
Preprint. Discussion started: 28 April 2026

Bonner, H. M., Raleigh, M. S., & Small, E. E. (2022). Isolating forest process effects on modelled snowpack density and snow water equivalent. *Hydrological Processes*, *36*(1), e14475. https://doi.org/10.1002/hyp.14475

Brangers, I., Marshall, H.-P., De Lannoy, G., Dunmire, D., Mätzler, C., & Lievens, H. (2024). Tower-based C-band radar measurements of an alpine snowpack. *The Cryosphere*, *18*(7), 3177–3193. https://doi.org/10.5194/tc-18-3177-2024

Brooks, P. D., Solomon, D. K., Kampf, S., Warix, S., Bern, C., Barnard, D., Barnard, H. R., Carling, G. T., Carroll, R. W. H., Chorover, J., Harpold, A., Lohse, K., Meza, F., McIntosh, J., Neilson, B., Sears, M., & Wolf, M. (2025). Groundwater dominates snowmelt runoff and controls streamflow efficiency in the western United States. *Communications Earth & Environment*, *6*(1), 1–8. https://doi.org/10.1038/s43247-025-02303-3

Buchhorn, M., Smets, B., Bertels, L., Roo, B. D., Lesiv, M., Tsendbazar, N.-E., Herold, M., & Fritz, S. (2020). *Copernicus Global Land Service: Land Cover 100m: collection 3: epoch 2019: Globe* [Dataset]. Zenodo. https://zenodo.org/records/3939050

California Department of Water Resources. (2025). *California Cooperative Snow Surveys (CCSS)* [Dataset]. https://cdec.water.ca.gov/snow/

Carletti, F., Marin, C., Ghielmini, C., Bavay, M., & Lehning, M. (2025). Multitemporal analysis of Sentinel-1 backscatter during snowmelt using high-resolution field measurements and radiative transfer modelling. *The Cryosphere*, *19*(11), 5579–5612. https://doi.org/10.5194/tc-19-5579-2025

Christopher-Moody, K. E. (2025). *EFFECTS OF FOREST MANAGEMENT ON SNOW ACCUMULATION AND ABLATION IN A MONTANE WATERSHED* [Montana State University - Bozeman, College of Letters & Science]. https://scholarworks.montana.edu/server/api/core/bitstreams/6faa1764-3b26-44b7-920e-838854eae520/content

Cortés, G., & Margulis, S. (2017). Impacts of El Niño and La Niña on interannual snow accumulation in the Andes: Results from a high-resolution 31 year reanalysis. *Geophysical Research Letters*, *44*(13), 6859–6867. https://doi.org/10.1002/2017GL073826

Cowherd, M., Mital, U., Rahimi, S., Girotto, M., Schwartz, A., & Feldman, D. (2024). Climate change-resilient snowpack estimation in the Western United States. *Communications Earth & Environment*, *5*(1), 1–10. https://doi.org/10.1038/s43247-024-01496-3

https://doi.org/10.5194/essd-2026-216
Preprint. Discussion started: 28 April 2026

Crumley, R. L., Palomaki, R. T., Nolin, A. W., Sproles, E. A., & Mar, E. J. (2020). SnowCloudMetrics: Snow Information for Everyone. *Remote Sensing*, *12*(20), Article 20. https://doi.org/10.3390/rs12203341

Darychuk, S. E., Shea, J. M., Menounos, B., Chesnokova, A., Jost, G., & Weber, F. (2023). Snowmelt characterization from optical and synthetic-aperture radar observations in the La Joie Basin, British Columbia. *The Cryosphere*, *17*(4), 1457–1473. https://doi.org/10.5194/tc-17-1457-2023

Dask Development Team. (2016). *Dask: Library for dynamic task scheduling* [Computer software]. http://dask.pydata.org

Dawson, N., Broxton, P., Zeng, X., Leuthold, M., Barlage, M., & Holbrook, P. (2016). An Evaluation of Snow Initializations in NCEP Global and Regional Forecasting Models. *Journal of Hydrometeorology*, *17*(6), 1885–1901. https://doi.org/10.1175/JHM-D-15-0227.1

Detre, A., McGrath, D., Gagliano, E., Bonnell, R., Webb, R., Marshall, H.-P., & Shean, D. (2025). Sentinel-1 SAR Estimates of Snowmelt Onset Coincide With SNOTEL Soil Moisture Pulses Across the Western United States. *Hydrological Processes*, *39*(12), e70341. https://doi.org/10.1002/hyp.70341

Dingman, S. L. (2015). *Physical Hydrology: Third Edition*. Waveland Press.

Dudley, R. W., Hodgkins, G. A., McHale, M. R., Kolian, M. J., & Renard, B. (2017). Trends in snowmelt-related streamflow timing in the conterminous United States. *Journal of Hydrology*, *547*, 208–221. https://doi.org/10.1016/j.jhydrol.2017.01.051

Fassnacht, S. R., Deitemeyer, D. C., & Venable, N. B. H. (2014). Capitalizing on the daily time step of snow telemetry data to model the snowmelt components of the hydrograph for small watersheds. *Hydrological Processes*, *28*(16), 4654–4668. https://doi.org/10.1002/hyp.10260

Fleming, S. W., Zukiewicz, L., Strobel, M. L., Hofman, H., & Goodbody, A. G. (2023). SNOTEL, the Soil Climate Analysis Network, and water supply forecasting at the Natural Resources Conservation Service: Past, present, and future. *JAWRA Journal of the American Water Resources Association*, *n/a*(n/a). https://doi.org/10.1111/1752-1688.13104

Frisbee, M. D., Phillips, F. M., Campbell, A. R., Liu, F., & Sanchez, S. A. (2011). Streamflow generation in a large, alpine watershed in the southern Rocky Mountains of Colorado: Is streamflow generation simply the aggregation of hillslope runoff responses? *Water Resources Research*, *47*(6). https://doi.org/10.1029/2010WR009391

https://doi.org/10.5194/essd-2026-216
Preprint. Discussion started: 28 April 2026

Gagliano, E. (2025a). *From Peak to Planet: Advancing Multi-Scale Detection of Snowmelt Timing with Satellite Radar* [Ph.D., University of Washington]. https://www.proquest.com/docview/3292774075/abstract/157792A913BD4CC2PQ/1

Gagliano, E. (2025b). *Global MODIS-derived seasonal snow cover (snow appearance date, disappearance date, and max consec snow days), water years 2015–2024* [Dataset]. Zenodo. https://doi.org/10.5281/zenodo.15692530

Gagliano, E. (2025c). *egagli/MODIS_seasonal_snow_mask: V1.0* [Computer software]. Zenodo. https://doi.org/10.5281/zenodo.17246166

Gagliano, E. (2026). *Global snowmelt runoff onset from Sentinel-1 SAR, 2015-2024* (Version 0.1) [Computer software]. https://github.com/egagli/global_snowmelt_runoff_onset

Gagliano, E., Shean, D., & Henderson, S. (2026). *A global high-resolution dataset of snowmelt runoff onset timing from Sentinel-1 SAR, 2015-2024* (Version 1.1.0) [Dataset]. Zenodo. https://doi.org/10.5281/zenodo.16953614

Gagliano, E., Shean, D., Henderson, S., & Vanderwilt, S. (2023). Capturing the Onset of Mountain Snowmelt Runoff Using Satellite Synthetic Aperture Radar. *Geophysical Research Letters*, *50*(21), e2023GL105303. https://doi.org/10.1029/2023GL105303

Gao, B., & Ma, W. (2024). Capturing Snowmelt Runoff Onset Date under Different Land Cover Types Using Synthetic Aperture Radar: Case Study of Sierra Nevada Mountains, USA. *Applied Sciences*, *14*(15), Article 15. https://doi.org/10.3390/app14156844

Gascoin, S., Lhermitte, S., Kinnard, C., Bortels, K., & Liston, G. E. (2013). Wind effects on snow cover in Pascua-Lama, Dry Andes of Chile. *Advances in Water Resources, Snow–Atmosphere Interactions and Hydrological Consequences*, *55*, 25–39. https://doi.org/10.1016/j.advwatres.2012.11.013

Hall, D., & Riggs, G. (2021). *MODIS/Terra Snow Cover 8-Day L3 Global 500m SIN Grid, Version 61* [Dataset]. NASA National Snow and Ice Data Center Distributed Active Archive Center. https://doi.org/10.5067/MODIS/MOD10A2.061

https://doi.org/10.5194/essd-2026-216
Preprint. Discussion started: 28 April 2026

Hoppinen, Z., Palomaki, R. T., Brencher, G., Dunmire, D., Gagliano, E., Marziliano, A., Tarricone, J., & Marshall, H.-P. (2024). Evaluating snow depth retrievals from Sentinel-1 volume scattering over NASA SnowEx sites. *The Cryosphere*, *18*(11), 5407–5430. https://doi.org/10.5194/tc-18-5407-2024

Ismail, M. F., Bogacki, W., Disse, M., Schäfer, M., & Kirschbauer, L. (2023). Estimating degree-day factors of snow based on energy flux components. *The Cryosphere*, *17*(1), 211–231. https://doi.org/10.5194/tc-17-211-2023

John, A., Ong, J., Theobald, E. J., Olden, J. D., Tan, A., & HilleRisLambers, J. (2020). Detecting Montane Flowering Phenology with CubeSat Imagery. *Remote Sensing*, *12*(18), Article 18. https://doi.org/10.3390/rs12182894

Johnson, J. B., & Schaefer, G. L. (2002). The influence of thermal, hydrologic, and snow deformation mechanisms on snow water equivalent pressure sensor accuracy. *Hydrological Processes*, *16*(18), 3529–3542. https://doi.org/10.1002/hyp.1236

Kaur, P., Webb, R., Tarricone, J., Rittger, K., McGrath, D., Gagliano, E., Palomaki, R., Bonnell, R., Forster, R., & Marshall, H. P. (in revision). *Feasibility Mapping of L-band InSAR for SWE retrievals*.

Kurum, M. (2015). C-Band SAR Backscatter Evaluation of 2008 Gallipoli Forest Fire. *IEEE Geoscience and Remote Sensing Letters*, *12*(5), 1091–1095. https://doi.org/10.1109/LGRS.2014.2382716

Lemmetyinen, J., Ruiz, J. J., Cohen, J., Haapamaa, J., Kontu, A., Pulliainen, J., & Praks, J. (2022). Attenuation of Radar Signal by a Boreal Forest Canopy in Winter. *IEEE Geoscience and Remote Sensing Letters*, *19*, 1–5. https://doi.org/10.1109/LGRS.2022.3187295

Lievens, H., Brangers, I., Marshall, H.-P., Jonas, T., Olefs, M., & De Lannoy, G. (2022). Sentinel-1 snow depth retrieval at sub-kilometer resolution over the European Alps. *The Cryosphere*, *16*(1), 159–177. https://doi.org/10.5194/tc-16-159-2022

Liston, G., & Sturm, M. (2021). *Global Seasonal-Snow Classification, Version 1*. NASA National Snow and Ice Data Center Distributed Active Archive Center. https://doi.org/10.5067/99FTCYYYLAQ0

Lowry, C. S., Deems, J. S., Loheide II, S. P., & Lundquist, J. D. (2010). Linking snowmelt-derived fluxes and groundwater flow in a high elevation meadow system, Sierra Nevada Mountains, California. *Hydrological Processes*, *24*(20), 2821–2833. https://doi.org/10.1002/hyp.7714

https://doi.org/10.5194/essd-2026-216
Preprint. Discussion started: 28 April 2026

Lund, J., Forster, R. R., Deeb, E. J., Liston, G. E., Skiles, S. M., & Marshall, H.-P. (2022). Interpreting Sentinel-1 SAR Backscatter Signals of Snowpack Surface Melt/Freeze, Warming, and Ripening, through Field Measurements and Physically-Based SnowModel. *Remote Sensing*, *14*(16), Article 16. https://doi.org/10.3390/rs14164002

Lund, J., Forster, R. R., Rupper, S. B., Deeb, E. J., Marshall, H. P., Hashmi, M. Z., & Burgess, E. (2020). Mapping Snowmelt Progression in the Upper Indus Basin With Synthetic Aperture Radar. *Frontiers in Earth Science*, *7*. https://www.frontiersin.org/articles/10.3389/feart.2019.00318

Lundquist, J. D., Cayan, D. R., & Dettinger, M. D. (2004). Spring Onset in the Sierra Nevada: When Is Snowmelt Independent of Elevation? *Journal of Hydrometeorology*, *5*(2), 327–342. https://doi.org/10.1175/1525-7541(2004)005%3C0327:SOITSN%3E2.0.CO;2

Lundquist, J. D., Dickerson-Lange, S. E., Lutz, J. A., & Cristea, N. C. (2013). Lower forest density enhances snow retention in regions with warmer winters: A global framework developed from plot-scale observations and modeling. *Water Resources Research*, *49*(10), 6356–6370. https://doi.org/10.1002/wrcr.20504

MacDonald, M., Fassnacht, S. R., & Tedesche, M. E. (2022). *High Elevation Post-Fire Landscapes on Snow Melt Trends in Seasonal and Transitional Snow Zones*. *2022*, GC53B-08. https://ui.adsabs.harvard.edu/abs/2022AGUFMGC53B..08M

Manickam, S., & Barros, A. (2020). Parsing Synthetic Aperture Radar Measurements of Snow in Complex Terrain: Scaling Behaviour and Sensitivity to Snow Wetness and Landcover. *Remote Sensing*, *12*(3), Article 3. https://doi.org/10.3390/rs12030483

Marin, C., Bertoldi, G., Premier, V., Callegari, M., Brida, C., Hürkamp, K., Tschiersch, J., Zebisch, M., & Notarnicola, C. (2020). Use of Sentinel-1 radar observations to evaluate snowmelt dynamics in alpine regions. *The Cryosphere*, *14*(3), 935–956. https://doi.org/10.5194/tc-14-935-2020

Matias, M. T., Ramage, J. M., Gurarie, E., & Brodzik, M. J. (2024). Snowmelt Onset and Caribou (Rangifer tarandus) Spring Migration. *Remote Sensing*, *16*(13), Article 13. https://doi.org/10.3390/rs16132391

Mätzler, C. (1987). Applications of the interaction of microwaves with the natural snow cover. *Remote Sensing Reviews*, *2*(2), 259–387. https://doi.org/10.1080/02757258709532086

https://doi.org/10.5194/essd-2026-216
Preprint. Discussion started: 28 April 2026

Meromy, L., Molotch, N. P., Link, T. E., Fassnacht, S. R., & Rice, R. (2013). Subgrid variability of snow water equivalent at operational snow stations in the western USA. *Hydrological Processes*, *27*(17), 2383–2400. https://doi.org/10.1002/hyp.9355

Microsoft Open Source, McFarland, M., Emanuele, R., Morris, D., & Augspurger, T. (2022). *microsoft/PlanetaryComputer: October 2022* (Version 2022.10.28) [Computer software]. Zenodo. https://doi.org/10.5281/zenodo.7261897

Mioduszewski, J. R., Rennermalm, A. K., Robinson, D. A., & Wang, L. (2015). Controls on Spatial and Temporal Variability in Northern Hemisphere Terrestrial Snow Melt Timing, 1979–2012. *Journal of Climate*, *28*(6), 2136–2153. https://doi.org/10.1175/JCLI-D-14-00558.1

Mirza, B. N., Small, E. E., & Raleigh, M. S. (2025). Evaluating the Utility of Sentinel-1 in a Data Assimilation System for Estimating Snow Depth in a Mountainous Basin. *EGUsphere*, 1–31. https://doi.org/10.5194/egusphere-2025-978

Musselman, K. N., Addor, N., Vano, J. A., & Molotch, N. P. (2021). Winter melt trends portend widespread declines in snow water resources. *Nature Climate Change*, *11*(5), Article 5. https://doi.org/10.1038/s41558-021-01014-9

Nagler, T. (1996). *Methods and analysis of synthetic aperture radar data from ERS-1 and X-SAR for snow and glacier applications* [Leopold-Franzens-Universität Innsbruck]. https://www.uibk.ac.at/projects/station-hintereis-opal-data/theses/pdf/nagler_1996.pdf

Nagler, T., Rott, H., Ripper, E., Bippus, G., & Hetzenecker, M. (2016). Advancements for Snowmelt Monitoring by Means of Sentinel-1 SAR. *Remote Sensing*, *8*(4), Article 4. https://doi.org/10.3390/rs8040348

Palomaki, R. T., & Sproles, E. A. (2023). Assessment of L-band InSAR snow estimation techniques over a shallow, heterogeneous prairie snowpack. *Remote Sensing of Environment*, *296*, 113744. https://doi.org/10.1016/j.rse.2023.113744

Pan, C. G., Kirchner, P. B., Kimball, J. S., & Du, J. (2021). *ABoVE: Passive Microwave-derived Annual Snowpack Main Melt Onset Date Maps, 1988-2023* (Version 1.0) [Dataset]. ORNL Distributed Active Archive Center. https://doi.org/https://doi.org/10.3334/ORNLDAAC/1841

https://doi.org/10.5194/essd-2026-216
Preprint. Discussion started: 28 April 2026

Pflug, J. M., Yang, K., Cristea, N., Boudreau, E. T., Vuyovich, C. M., & Kumar, S. V. (2024). Using Commercial Satellite Imagery to Reconstruct 3 m and Daily Spring Snow Water Equivalent. *Water Resources Research*, *60*(11), e2024WR037983. https://doi.org/10.1029/2024WR037983

Potin, P., Colin, O., Pinheiro, M., Rosich, B., O'Connell, A., Ormston, T., Gratadour, J.-B., & Torres, R. (2022). Status And Evolution Of The Sentinel-1 Mission. *IGARSS 2022 - 2022 IEEE International Geoscience and Remote Sensing Symposium*, 4707–4710. https://doi.org/10.1109/IGARSS46834.2022.9884753

Qin, Y., Hong, C., Zhao, H., Siebert, S., Abatzoglou, J. T., Huning, L. S., Sloat, L. L., Park, S., Li, S., Munroe, D. K., Zhu, T., Davis, S. J., & Mueller, N. D. (2022). Snowmelt risk telecouplings for irrigated agriculture. *Nature Climate Change*, *12*(11), 1007–1015. https://doi.org/10.1038/s41558-022-01509-z

Raleigh, M. S., Gutmann, E. D., Van Stan II, J. T., Burns, S. P., Blanken, P. D., & Small, E. E. (2022). Challenges and Capabilities in Estimating Snow Mass Intercepted in Conifer Canopies With Tree Sway Monitoring. *Water Resources Research*, *58*(3), e2021WR030972. https://doi.org/10.1029/2021WR030972

Réveillet, M., MacDonell, S., Gascoin, S., Kinnard, C., Lhermitte, S., & Schaffer, N. (2020). Impact of forcing on sublimation simulations for a high mountain catchment in the semiarid Andes. *The Cryosphere*, *14*(1), 147–163. https://doi.org/10.5194/tc-14-147-2020

Rickenbaugh, L., Sproles, E., Gagliano, E., Covino, T., Tuholske, C., & Carroll, R. W. H. (2026). When and where does water originate? Leveraging stable water isotopes and Synthetic Aperture Radar to assess the hydrology of a snow-dominated watershed in Southwestern Montana. *Remote Sensing Applications: Society and Environment*, 101887. https://doi.org/10.1016/j.rsase.2026.101887

Rott, H., & Nagler, T. (1995). Monitoring temporal dynamics of snowmelt with ERS-1 SAR. *1995 International Geoscience and Remote Sensing Symposium, IGARSS '95. Quantitative Remote Sensing for Science and Applications*, *3*, 1747–1749. https://doi.org/10.1109/IGARSS.1995.524014

Royer, A., Picard, G., Vargel, C., Langlois, A., Gouttevin, I., & Dumont, M. (2021). Improved Simulation of Arctic Circumpolar Land Area Snow Properties and Soil Temperatures. *Frontiers in Earth Science*, *9*. https://doi.org/10.3389/feart.2021.685140

https://doi.org/10.5194/essd-2026-216
Preprint. Discussion started: 28 April 2026

Saavedra, F. A., Kampf, S. K., Fassnacht, S. R., & Sibold, J. S. (2017). A snow climatology of the Andes Mountains from MODIS snow cover data. *International Journal of Climatology*, *37*(3), 1526–1539. https://doi.org/10.1002/joc.4795

Skiles, S. M., Flanner, M., Cook, J. M., Dumont, M., & Painter, T. H. (2018). Radiative forcing by light-absorbing particles in snow. *Nature Climate Change*, *8*(11), 964–971. https://doi.org/10.1038/s41558-018-0296-5

Steele-Dunne, S. C., Friesen, J., & van de Giesen, N. (2012). Using Diurnal Variation in Backscatter to Detect Vegetation Water Stress. *IEEE Transactions on Geoscience and Remote Sensing*, *50*(7), 2618–2629. https://doi.org/10.1109/TGRS.2012.2194156

Sturm, M., Holmgren, J., & Liston, G. E. (1995). A Seasonal Snow Cover Classification System for Local to Global Applications. *Journal of Climate*, *8*(5), 1261–1283. https://doi.org/10.1175/1520-0442(1995)008%3C1261:ASSCCS%3E2.0.CO;2

Tang, Z., Deng, G., Hu, G., Zhang, H., Pan, H., & Sang, G. (2022). Satellite observed spatiotemporal variability of snow cover and snow phenology over high mountain Asia from 2002 to 2021. *Journal of Hydrology*, *613*, 128438. https://doi.org/10.1016/j.jhydrol.2022.128438

Tarricone, J., Webb, R. W., Marshall, H.-P., Nolin, A. W., & Meyer, F. J. (2023). Estimating snow accumulation and ablation with L-band interferometric synthetic aperture radar (InSAR). *The Cryosphere*, *17*(5), 1997–2019. https://doi.org/10.5194/tc-17-1997-2023

Tsai, Y.-L. S., Dietz, A., Oppelt, N., & Kuenzer, C. (2019). Remote Sensing of Snow Cover Using Spaceborne SAR: A Review. *Remote Sensing*, *11*(12), Article 12.

USDA Natural Resources Conservation Service. (2022). *SNOwpack TELemetry Network (SNOTEL)* [Dataset]. https://data.nal.usda.gov/dataset/snowpack-telemetry-network-snotel

Webb, R. W., Fassnacht, S. R., & Gooseff, M. N. (2017). Defining the Diurnal Pattern of Snowmelt Using a Beta Distribution Function. *JAWRA Journal of the American Water Resources Association*, *53*(3), 684–696. https://doi.org/10.1111/1752-1688.12522

https://doi.org/10.5194/essd-2026-216
Preprint. Discussion started: 28 April 2026

930 Wrzesien, M. L., Pavelsky, T. M., Durand, M. T., Dozier, J., & Lundquist, J. D. (2019). Characterizing Biases in Mountain Snow Accumulation From Global Data Sets. *Water Resources Research*, *55*(11), 9873–9891. https://doi.org/10.1029/2019WR025350

Yang, T., Li, Q., Zou, Q., Hamdi, R., Cui, F., & Li, L. (2022). Impact of Snowpack on the Land Surface Phenology in the Tianshan Mountains, Central Asia. *Remote Sensing*, *14*(14), Article 14. https://doi.org/10.3390/rs14143462

935 Zheng, L., Cheng, X., Chen, Z., Wang, S., Liang, Q., & Wang, K. (2022). Global Snowmelt Onset Reflects Climate Variability: Insights from Spaceborne Radiometer Observations. *Journal of Climate*, *35*(10), 2945–2959. https://doi.org/10.1175/JCLI-D-21-0265.1